



Influence of basement rocks on fluid evolution during multiphase deformation: the example of the Estamariu thrust in the Pyrenean Axial Zone

Daniel Muñoz-López¹, Gemma Alías¹, David Cruset², Irene Cantarero¹, Cédric M. Jonh³, Anna Travé¹

5 ¹Department de Mineralogia, Petrologia i Geologia Aplicada. Facultat de Ciències de la Terra, Universitat de Barcelona (UB), C/ Martí i Franquès s/n, 08028 Barcelona, Spain.

²Institut de Ciències de la Terra Jaume Almera, ICTJA-CSIC, Lluís Solé i Sabarís s/n, 08028 Barcelona, Spain.

³ Department of Earth Science and Engineering, Imperial College London, London SW7 2BP, UK.

10 *Correspondence to:* Daniel Muñoz-López (munoz-lopez@ub.edu)

Abstract. Calcite veins precipitated in the Estamariu thrust during two tectonic events decipher the temporal and spatial relationships between deformation and fluid migration in a long-lived thrust and determine the influence of basement rocks on the fluid chemistry during deformation. Structural and petrological observations constrain the timing of fluid migration and vein formation, whilst geochemical analyses ($\delta^{13}\text{C}$, $\delta^{18}\text{O}$, $^{87}\text{Sr}/^{86}\text{Sr}$, clumped isotope thermometry and elemental composition) of the related calcite cements and host rocks indicate the fluid origin, pathways and extent of fluid-rock interaction. The first tectonic event, recorded by calcite cements Cc1a and Cc2, is related to the Alpine reactivation of the Estamariu thrust, and is characterized by the migration of meteoric fluids, heated at depth (temperatures between 56 and 98 °C) and interacted with crystalline basement rocks before upflowing through the thrust zone. During the Neogene extension, the Estamariu thrust was reactivated and normal faults and shear fractures with calcite cements Cc3, Cc4 and Cc5 developed. Cc3 and Cc4 precipitated from hydrothermal fluids (temperatures between 127 and 208 °C and between 102 and 167 °C, respectively) derived from crystalline basement rocks and expelled through fault zones during deformation. Cc5 precipitated from low temperature meteoric waters percolating from the surface through small shear fractures. The comparison between our results and already published data in other structures from the Pyrenees suggests that regardless of the origin of the fluids and the tectonic context, basement rocks have a significant influence on the fluid chemistry, particularly on the $^{87}\text{Sr}/^{86}\text{Sr}$ ratio. Accordingly, the cements precipitated from fluids interacted with crystalline basement rocks have significantly higher $^{87}\text{Sr}/^{86}\text{Sr}$ ratios (> 0.710) with respect to those precipitated from fluids that have interacted with the sedimentary cover (< 0.710).

1 Introduction

Deformation associated with crustal shortening is mainly accommodated by thrust faulting and related fault zone structures. Successive faulting may occur and favourably oriented structures may undergo reactivation during different tectonic events in a long-lived orogenic belt (Cochelin et al., 2018; Sibson, 1995). The reactivation of faults may produce changes in the hydraulic



behaviour of fault zones as well as in the origin and regime of fluids circulating through them. Consequently, constraining the timing of deformation and fluid migration is essential to better understand the current configuration of a mountain belt, its evolution through time and the mobilization of different fluids during successive deformation events (Baqués et al., 2012; Crespo-Blanc et al., 1995; Faj-Gomord et al., 2018; Fitz-Diaz et al., 2011; Lacroix et al., 2014). Understanding basin-scale
35 fluid flow is of primary importance to reconstruct the diagenetic history of a sedimentary basin, as fluids take part in a wide range of geological processes including precipitation of new mineral phases, dolomitization and petroleum migration, among others (Barker et al., 2009; Foden, 2001; Fontana et al., 2014; Gomez-Rivas et al., 2014; Martín-Martín et al., 2015; Mozafari et al., 2019; Piessens et al., 2002). Due to the economic interest of these processes, in particular related to oil and ore deposits
40 exploration, CO₂ sequestration, seismic activity and water management, many researchers have addressed the study of the relationship between deformation and fluid migration (Beaudoin et al., 2014; Breesch et al., 2009; Cox, 2007; Dewever et al., 2013; Gasparri et al., 2013; Suchy et al., 2000; Travé et al., 2009; Voicu et al., 2000; Warren et al., 2014).

In the Pyrenees, the crystalline basement rocks from the Axial Zone are affected by numerous fault systems considered Variscan in age but reactivated during the Pyrenean compression (Cochelin et al., 2018; Poblet, 1991). However, no real consensus exists about the influence of the Alpine deformation on the basement rocks and the age of basement-involved
45 structures is still debated (Cochelin et al., 2018; García-Sansegundo et al., 2011). As a consequence, the relationships between deformation and fluid flow have been focused on structures from the Mesozoic and Cenozoic cover (Crogner et al., 2018; Cruset et al., 2016, 2018; Beaudoin et al., 2015; Lacroix et al., 2011, 2014; Nardini et al., 2019; Travé et al., 1997, 1998, 2000, 2007), where the timing of deformation and thrust emplacement is well-constrained (Vergés et al., 2002; Vergés, 1993; Vergés and Muñoz, 1990). Contrarily, only a few contributions, concentrated along the Gavarnie thrust system, have tackled this topic
50 in the Paleozoic basement involving crystalline rocks (Banks et al., 1991; Grant et al., 1990; Henderson and McCaig, 1996; McCaig et al., 2000a, 1995; Rye and Bradbury, 1988; Trincal et al., 2017). On the other hand, another important aspect of studying the fault-fluid system is related to the heat flow and the influence of faults on the development of geothermal systems (Faulds et al., 2010; Grasby and Hutcheon, 2001; Liotta et al., 2010; Rowland and Sibson, 2004). Particularly, in the NE part of the Iberian Peninsula (including the Pyrenees and the Catalan Coastal Ranges), the presence of high-permeability Neogene
55 extensional faults, acting as conduits for focused upward migration, provide efficient pathways for hydrothermal fluids to flow from deeper to shallower crustal levels (Carmona et al., 2000; Fernández and Banda, 1990; Taillefer et al., 2017, 2018). In this sense, understanding the fault-fluid system evolution and the timing of hydrothermal fluid migration is of great importance to characterize the potential geothermal resources of this area.

In this contribution, we report the temporal and spatial relationships between deformation and fluid migration in a long-lived
60 Variscan thrust deforming basement rocks in the Pyrenean Axial Zone. For this purpose, we combine structural, petrological and geochemical analyses of calcite veins precipitated in the Estamariu thrust during two episodes of regional tectonic activity (Pyrenean compression and Neogene extension). Structural and petrological observations allow us to unravel the timing of fluid migration and vein formation in relation to the involved tectonic events. The geochemistry of the vein cements and related host rocks provides information on the fluid origin, pathways and extent of fluid-rock interaction during deformation. The



65 integration of all these data within the studied geological setting in the Pyrenean basement will allow us: (i) to constrain the timing of vein formation and fluid migration; (ii) to determine the fluid origin and pathways during successive compressional and extensional deformation phases; (iii) to assess the influence of basement rocks on the chemistry of fluids circulating during deformation; and (iv) to provide insights into the fluid flow at regional scale in the NE part of the Iberian Peninsula, where the presence of hydrothermal fluids has been reported from Neogene times to present.

70 **2 Geological setting**

The Pyrenees constitute an asymmetric and doubly verging orogenic belt developed from the Late Cretaceous to Oligocene in relation to the Alpine convergence between the Iberian and European plates (Choukroune, 1989; Muñoz, 1992; Roure et al., 1989; Sibuet et al., 2004; Srivastava et al., 1990; Vergés and Fernández, 2012). The Pyrenean structure consists of a central antiformal stack of basement-involved rocks from the Axial Zone, flanked by two oppositely verging fold-and-thrust belts and their associated foreland basins (Muñoz, 1992; Muñoz et al., 1986) (Fig. 1A). The Axial Zone represents a fragment of the European Variscan orogeny incorporated into the Pyrenean belt during the Alpine convergence (Matte, 1991). It consists of a duplex of three south-directed basement thrust sheets (from upper to lower: Noguères, Orri and Rialp), involving Cambrian to Carboniferous rocks deformed by the Variscan compressional events, and an Upper Carboniferous to Triassic post-Variscan cover (Poblet, 1991; Saura, 2004; Saura and Teixell, 2006).

80 During the Neogene tectonic evolution of the eastern Axial Pyrenees, a horst and basin system bounded by E-W to ENE-WSW faults developed (Roca, 1996; Roca and Guimerà, 1992). The most important fault, La Tet fault (roughly striking N60°E and dipping around 60°N) has associated a set of E-W extensional basins such as La Cerdanya, Conflent, La Seu d'Urgell and Cerc basins (Cabrera et al., 1988; Roca, 1996). The Cerc basin consists of a Stephano-Permian accumulation of volcanic rocks discordantly overlying Cambro-Ordovician materials from the Orri thrust sheet. This basin is thrust in its eastern limit by the Estamariu thrust, whereas the northern and southern boundaries correspond to two Neogene extensional faults, La Seu d'Urgell fault and the Ortedó fault, respectively (Hartevelt, 1970; Roca, 1996; Saura, 2004) (Fig. 1B, C). In the NW part of the basin, the limit between the Stephano-Permian unit and the Upper Ordovician sequence corresponds to a Stephano-Permian extensional fault formed coevally with the deposition of the volcanic sequence (Saura, 2004). This fault was reactivated during the latest stages of the Neogene extension (Saura, 2004) and is here referred as the Sant Antoni fault (Fig. 1C).

90 The Estamariu thrust is a basement-involved reverse fault originated during the Variscan orogeny with a minimum displacement of 27 km (Poblet, 1991). However, in its southwestern termination, it juxtaposes the Devonian Rueda Formation against the Stephano-Permian Erill Castell Formation. The Erill Castell Formation developed during the late to post-orogenic collapse of the Variscan belt (Lago et al., 2004; Ziegler, 1988), evidencing the reactivation of the Estamariu thrust during the Alpine Orogeny (Poblet, 1991; Saura, 2004).

95 Rocks cropping out around the Estamariu thrust and the Cerc basin range from Upper Ordovician to Miocene (Fig. 1C) and are deformed by successive Variscan, Alpine and Neogene phases (Saura and Teixell, 2006). Due to such a complex structural



100 setting, the stratigraphic record is discontinuous and only Upper Ordovician, Devonian, Stephano-Permian and Neogene successions are present in the study area. The Upper Ordovician consists mainly of a detrital sedimentary sequence affected by a low-graded metamorphism (Hartevelt, 1970; Poblet, 1991; Saura, 2004). This succession basically includes a centimetric to metric alternation of shales, sandstones, conglomerates, quartzites and phyllites. The Devonian succession consists of a centimetric to decimetric alternation of limestones and black slates (Rueda Formation) (Mey, 1967). The Stephano-Permian sequence is represented by a volcanic and volcanoclastic unit (the Erill Castell Formation) (Mey et al., 1968), involving tuffs and ignimbrites at the base and andesites in the upper part (Martí, 1996; Saura and Teixell, 2006). Finally, the Neogene sequence is constituted of detrital and poorly lithified sediments, mainly shales, sandstones and conglomerates (Roca, 1996).

105 3 Methods

This study integrates a field compilation of structural data and samples and petrological and geochemical analyses of calcite cements and related host rocks. The structural data includes bedding, foliation strike and fracture orientation, type, crosscutting relationships and kinematics. Such data were plotted in equal-area lower-hemisphere projections and integrated in a schematic map and a cross-section of the Estamariu thrust and the Cerc basin (Fig. 2A, B and 3). Host rocks and calcite cements were 110 sampled for petrological and geochemical analyses. Thin sections were studied under a Zeiss Axiophot optical microscope and a Cold cathodoluminescence (CL) microscope model 8200 Mk5-1 operating between 16–19 kV and 350 μ A gun current. Thirty-five representative samples of the different generations of calcite cements and the carbonate portion of the Devonian rocks were sampled for carbon and oxygen isotopy. Sampling was carried out with a 500 μ m-diameter microdrill. 50-100 μ g of powdered samples were reacted with 100% phosphoric acid during two minutes at 70 °C. The resultant CO₂ was analyzed 115 with an automated Kiel Carbonate Device attached to a Thermal Ionization Mass Spectrometer Thermo Electron MAT-252 (Thermo Fisher Scientific) according to the method of McCrea (1950). For calibration, the International Standard NBS-18 and the internal standard RC-1, traceable to the International Standard NBS-19, were used. The standard deviation is $\pm 0.03\%$ for $\delta^{13}\text{C}$ and $\pm 0.05\%$ for $\delta^{18}\text{O}$ expressed with respect to the VPDB standard (Vienna Pee Dee Belemnite).

The elemental composition of twelve samples of calcite cements and related host rocks were analyzed using a high resolution 120 inductively coupled plasma-mass spectrometry (HR-ICP-MS, model Element XR, Thermo Fisher Scientific). 100 mg of powdered samples were dried at 40 °C during 24 h and then, they were acid digested in closed polytetrafluoroethylene (PTFE) vessels with a combination of HNO₃ + HF + HClO₄ (2.5 mL: 5 mL: 2.5 mL v/v). The samples were evaporated and 1 mL of HNO₃ was added to make a double evaporation. Finally, the samples were re-dissolved and diluted with MilliQ water (18.2 M Ω cm⁻¹) and 1 mL of HNO₃ in a 100 mL volume flask. A tuning solution containing 1 g L⁻¹ Li, B, Na, K, Sc, Fe, Co, Cu, 125 Ga, Y, Rh, In, Ba, Tl, U was used in order to improve the sensitivity of the ICP-MS, and as internal standard, 20 mg L⁻¹ of a monoelemental solution of ¹¹⁵In. Reference materials are the BCS-CRM n° 393 (ECRM 752-1) limestone, JA-2 Andesite and JB-3 Basalt. The precision of the results was expressed in terms of two standard deviations of a set of eight reference materials measurements (reference material JA-2), whereas accuracy (%) was calculated using the absolute value of the difference



130 between the measured values obtained during the analysis and the certified values of a set of eight reference material analysis (reference material BCS-CRM n° 393 for major oxides and JA-2 for trace elements). The detection limit (DL) was calculated as three times the standard deviation of the average of ten blanks.

The $^{87}\text{Sr}/^{86}\text{Sr}$ ratio was analyzed for eight representative samples of calcite cements and host rocks. Powdered samples were dissolved in 5 mL of 10% acetic acid. After centrifugation, the supernatant was dried and dissolved in 1 mL of 1M HNO_3 . The solid residue generated after evaporation was diluted in 3 mL of 3M HNO_3 and loaded into chromatographic columns to
135 separate the Rb-free Sr fraction, using SrResinTM (crown-ether (4,4'(5')-di-t-butylcyclohexano-18-crown-6)) and 0.05M HNO_3 as eluent. After evaporation, samples were loaded onto a Re filament along with 1 μL of 1 M phosphoric acid and 2 μL of Ta_2O_5 . Isotopic analyses were carried out in a TIMS-Phoenix mass spectrometer performing a dynamic multicollection method, during 10 blocks of 16 cycles each one, keeping a ^{88}Sr beam intensity of 3-V. Possible ^{87}Rb interferences and possible mass fractionation during sample loading and analysis were corrected and normalized with the reference value of $^{88}\text{Sr}/^{86}\text{Sr} =$
140 0.1194. The isotopic standard NBS-987 was analyzed six times during sample analysis, yielding an average value of 0.710243 ± 0.000009 (standard deviation, 2σ). NBS 987 data have been used to correct the sample ratios for standard drift from the certified value. The analytical error in the $^{87}\text{Sr}/^{86}\text{Sr}$ ratio, referred to two standard deviations, was 0.01%, whereas the internal precision is 0.000003. Sr procedural blanks were always below 0.5 ng.

The $^{143}\text{Nd}/^{144}\text{Nd}$ ratios were analyzed in seven samples of calcite cements and host rocks. Samples were weighted in Teflon[®]
145 vessels, with enriched spike solution (^{149}Sm - ^{150}Nd - Oak Ridge) and dissolved in 5 mL of ultrapure HF and 3 mL of ultrapure HNO_3 (Merck-SuprapurTM). The PFA-vessels were placed 65 hours at 120 °C into an oven. After that, cold vials were evaporated at 120 °C on a heat plate. 4 mL of 6N distilled HCL were added to the dried samples and placed at 120 °C in an oven overnight. The solid residue generated after evaporation was dissolved in 3 mL of distilled and titrated 2.5 N HCl. Samples were centrifuged at 4000 rpm for 10 minutes to separate the possible dissolved fraction from the residue.
150 Chromatographic separation of the whole group of REE was performed with a previously calibrated cation exchange resin DOWEX 50W-X8 200-400 mesh. After that, recovered REE fractions were dried and again dissolved in 200 μL HCl 0.18N. Such solutions were passed in a new chromatographic step (Ln-resin). The result is a complete separation between the Nd and the Sm fractions, using 0.3N HCl and 0.4N HCl as eluent, respectively. Dried Sm and Nd samples dissolved with 2 μL of 0.05M phosphoric acid were loaded onto a side Rhenium (Re) filament of a triple Re filament arrangement. Nd ratios were
155 analysed in a mass spectrometer TIMS-Phoenix[®], using a dynamic multicollection method, through 160 cycles at a stable intensity of 1V for the ^{144}Nd mass. In turn, Sm ratios were analysed in the same spectrometer, using a single static method through 112 cycles keeping 1V intensity for the ^{149}Sm mass. Nd analyses were corrected for ^{142}Ce and ^{144}Sm interferences, if any, and normalized to a ratio of $^{146}\text{Nd}/^{144}\text{Nd} = 0.7219$ to correct the possible mass fractionation during the processes of loading and analysing at the TIMS. Nd isotopic standard JNdi-1 was checked to correct the sample ratios for standard drift from the
160 certified value. The analytical error (2STD) was 0.1% in the $^{147}\text{Sm}/^{144}\text{Nd}$ ratio and 0.006% in the $^{143}\text{Nd}/^{144}\text{Nd}$ ratio. Procedural blanks were always below 0.1 ng.



U-Pb geochronology of the calcite cements Cc1a to Cc5 was accomplished at FIERCE (Frankfurt Isotope and Element Research Center, Goethe University) using a laser ablation inductively coupled plasma mass spectrometry (LA-ICPMS). Clumped isotope thermometry of the calcite cements was carried out in order to determine the temperature and composition ($\delta^{18}\text{O}_{\text{fluid}}$) of the vein-forming fluids. 2–3 mg aliquots from cements were measured with an automated line, the Imperial Batch Extraction system (IBEX), developed at Imperial College. Samples were dropped in 105% phosphoric acid at 90 °C and reacted during 30 min. The reactant CO_2 was separated with a poropak-Q column and transferred into the bellows of a Thermo Scientific MAT 253 mass spectrometer. The characterization of a replicate consisted of 8 acquisitions in dual inlet mode with 7 cycles per acquisition. The post-acquisition processing was completed with Easotope, a software for clumped isotope analyses (John and Bowen, 2016). During phosphoric acid digestion, Δ_{47} values were corrected for isotope fractionation using a phosphoric acid correction of 0.069‰ at 90 °C for calcite (Guo et al., 2009). The data were also corrected for non-linearity applying the heated gas method (Huntington et al., 2009) and projected into the reference frame of Dennis et al., (2011). Carbonate $\delta^{18}\text{O}$ values were calculated with the acid fractionation factors of Kim and O’Neil, (1997). Results were converted to temperatures applying the calibration method of Kluge et al., (2015). Calculated $\delta^{18}\text{O}_{\text{fluid}}$ values are expressed in ‰ with respect to the Vienna Standard Mean Ocean Water (VSMOW).

4 Results

4.1 Structure and associated calcite cements

The Estamariu thrust strikes N-S to NW-SE and dips between 40 and 70° towards the NE. It has a displacement of a few hundred meters and juxtaposes a Devonian alternation of limestones and shales in the hanging wall against Stephano-Permian andesites in the footwall (Poblet, 1991) (Fig. 2-4). The main slip plane is undulose, producing changes in the strike direction and dip, and generates a 2 – 3 m thick thrust zone, which is thicker in the hanging wall, up to 2.5 m thick. In the footwall, the thrust zone is less than 1 m thick and has associated minor restricted thrust zones developed as subsidiary accommodation structures related to the main thrust fault (Fig. 2A, B). All kinematic indicators, including S-C structures and slickenlines, indicate reverse displacement towards the west.

The mesostructures and microstructures observed in the study area are described below according to their structural position in relation to the Estamariu thrust, that is, hanging wall, thrust zone and footwall (Fig. 3, 4).

In the studied outcrops, the Devonian Rueda Formation from the hanging wall is characterized by a well-bedded alternation of dark to light grey limestones with dark grey shales (Fig. 5A). Limestones are more abundant and are made up of encrinites, which consist of a bioclastic packstone formed essentially of crinoid stems (Fig. 5B). Under cathodoluminescence, encrinites show dark to bright orange colors (Fig. 5C). Deformation in the Devonian protolith (i.e., outside the thrust zone) corresponds to a decametric anticline (Fig. 2B), which has associated an axial plane pervasive regional foliation (Sr) concentrated in the pelitic intervals (Fig. 5B). The Sr has a NW-SE mean orientation, dips 30 to 55° towards the E and NE and is generally between



2 and 5 cm spaced. The angular relationship between the Devonian bedding strike and the regional foliation is oblique and changes to nearly perpendicular when approaching the thrust zone (Fig. 2B).

195 Within the thrust zone affecting the hanging wall, the Devonian host rocks are still recognizable, but deformation intensity progressively increases towards the main thrust plane. This deformation consists of a penetrative thrust zone foliation (S_D), two generations of stylolites (e1, e2) and three generations of calcite veins (V0, V1a and V1b) (Fig. 3, 6). These structures are described below in chronological order.

200 The foliation within the thrust zone affecting the Devonian hanging wall strikes NW-SE and dips 40 – 50° NE, similar to the regional foliation in the protolith, but it is more closely spaced, generally between 0.2 and 1 cm (Fig. 6A, B). This observation points out to a progressive transposition of the regional foliation within the thrust zone during thrusting. At mesoscale, S_D has related shear surfaces (Ci) defining centimetric S-C-type structures, again indicating reverse kinematics (Fig. 6A).

Stylolites e1 have a wave-like shape and trend subparallel to the thrust zone foliation (Fig. 6B, C). When present, these stylolites are very systematic with densities between 5 and 8 stylolites/cm.

205 The first calcite vein generation (V0), only observed at microscopic scale (Fig. 6B, C), corresponds to up to 1 cm long and less than 1 mm thick veins cemented by blocky to elongate blocky calcite crystals featuring a dark-brown luminescence (cement Cc0). Veins V0 and stylolites e1 are perpendicular between them and show ambiguous crosscutting relationships. These microstructures are concentrated into discontinuous fragments of the Devonian host rocks within the thrust zone. Calcite veins V1a crosscut the previous vein generation (V0) and are developed within S_D surfaces (Fig. 3, 6D). These veins are the most
210 abundant, exhibit a white to brownish color in hand sample and are up to 10 cm long and 1 cm thick. The vein cement (Cc1a) is formed of up to 3-4 mm in size anhedral crystals displaying a blocky texture and a dark brown luminescence (Fig. 6E).

Stylolites e2, more abundant than stylolites e1, are up to 10 cm long and show spacing between 0.5 and 2 cm (Fig. 6D, F). These stylolites mainly correspond to sutured areas developed between the host rock and the calcite veins V1a and between foliation surfaces.

215 Calcite veins V1b, up to 1 cm long and less than one mm thick, were also identified at microscopic scale (Fig. 6D, F). The vein cement (Cc1b) consists of up to 0.1 mm calcite crystals with a blocky texture and a bright yellow luminescence. These veins postdate the previous V0 and V1a generations and trend perpendicular to stylolites e2.

Towards the fault plane, the thrust zone foliation is progressively more closely-spaced and stylolites e2 become more abundant (showing mm spacing) and exhibit ambiguous cross-cutting relationships with veins V1b (Fig. 6F). The main slip surface
220 corresponds to a discrete plane that contains calcite slickensides (veins V2). The vein cement (Cc2) is milky white in hand sample and consists of up to 3 mm blocky to elongated blocky crystals (Fig. 6G) with a dull to bright orange luminescence (Fig. 6H).

Deformation in the footwall is concentrated within the main thrust zone and subsidiary thrust zones and corresponds to a thrust zone foliation (S_{SP}) and calcite veins V3 (Fig. 3).

225 The foliation strikes NW-SE, dips towards the NE and is mm to cm spaced (Fig. 7A). Calcite veins V3 are generally 1 – 2 cm thick and strike NW-SE. They are parallel or locally branch off cutting the foliation planes in the subsidiary thrust zone (Fig.



7A, B). Outside the thrust zone, veins V3 are locally present but have a NE-SW strike. These veins are mostly less than 1 m long and are spaced between a few cm and 50 cm. The vein cement (Cc3) is made up of a milky white calcite characterized by up to 3 mm long fibrous crystals oriented perpendicular to the vein walls (Fig. 7C). Locally, anhedral blocky crystals ranging in size from 0.1 to 1 mm are also present. This cement displays a bright yellow to bright orange luminescence (Fig. 7D).

In the footwall, the Stephano-Permian Erill Castell Formation comprises massive, dark-greenish andesitic levels showing a rhythmic magmatic layering (Sm) (Fig. 7E), which corresponds to a fluidal structure of the host rock. The local presence of pyroclastic and brecciated volcanoclastic levels is also ubiquitous mainly in the lower part of this sequence. Andesites are characterized by a porphyritic texture defined by a dark fine-grained spherulitic matrix partially devitrified and large zoned crystals of plagioclase (Fig. 7F), up to 2 – 3 cm long, and less abundant biotite and hornblende. These mafic phenocrysts are systematically pseudomorphosed by clay minerals and frequently show evidence of oxidation and chloritization. Andesites are affected by E-W striking open joints (J1) dipping indistinctively towards the north and south (Fig. 7E). These joints locally trend parallel to the magmatic layering (Fig. 3).

Finally, as described above, the northern and southern limits of both the Cerc basin and the Estamariu thrust correspond to two Neogene extensional faults, La Seu d'Urgell and the Ortedó fault systems (Fig 1C). These faults are subvertical or greatly dip towards the north. In the northern part, the slip plane of La Seu d'Urgell fault has not been observed and the limit between the Stephano-Permian rocks and the Neogene deposits is not well constrained due to the poor quality of the Neogene outcrops and the presence of Quaternary deposits. In the southern part, the Ortedó fault generates a several meter-thick dark greyish to brown fault zone, characterized by the presence of clay-rich incohesive fault rocks developed at the contact between Stephano-Permian and Upper Ordovician rocks. Related to these main fault systems, mesoscale normal faults (V4) are also frequent affecting the andesites within the Cerc basin. These faults are mainly E-W and locally NE-SW, are subvertical and dip indistinctly towards the N and S. Fault planes are locally mineralized with calcite cement and exhibit two striae set generations indicating dip-slip and strike-slip movements (Fig. 8A). The calcite cement (Cc4) consists of up to 2 mm blocky to elongated blocky crystals (Fig. 8B) with a homogeneous dark orange luminescence (Fig. 8C). On the other hand, the main Estamariu thrust zone is locally displaced by shear fractures (V5) (Fig. 8D) and a later set of shear bands (Cn) (Fig. 8E), both having an overall NNW-SSE to NNE-SSW strike (Fig. 3) that indicate a minor normal displacement. Shear fractures (V5) are locally mineralized with a greyish microsparite calcite cement (Cc5).

4.2 Geochemistry of calcite cements and host rocks

The geochemistry ($\delta^{18}\text{O}$, $\delta^{13}\text{C}$, $\delta^{18}\text{O}_{\text{fluid}}$, $^{87}\text{Sr}/^{86}\text{Sr}$, $^{143}\text{Nd}/^{144}\text{Nd}$ and elemental composition) and the calculated temperature of precipitation of the different calcite cements Cc1a to Cc5 are described below. Veins V0 and V1b were only observed at microscopic scale and their calcite cement Cc0 and Cc1b could not be sampled to perform these geochemical analyses.

The $\delta^{18}\text{O}$ and $\delta^{13}\text{C}$ isotopic composition of the carbonate fraction of the Devonian hanging wall and the different calcite cements (Cc1a to Cc5) are summarized in Table 1 and represented in Fig. 9. The micritic matrix of the Devonian packstone



260 ranges in $\delta^{18}\text{O}$ values between -10.5 and -8.4 ‰VPDB and in $\delta^{13}\text{C}$ values between +1.5 and +2.8 ‰VPDB, whereas the calcite cements have a broader range of values depending on the cement generation (Fig. 9).

Calcite cement Cc1a has $\delta^{18}\text{O}$ values between -11.3 and -10.3 ‰VPDB and $\delta^{13}\text{C}$ values between +0.8 and +2.1 ‰VPDB. Cc2 is characterized by $\delta^{18}\text{O}$ values between -14.9 and -12.9 ‰VPDB and $\delta^{13}\text{C}$ values between -1.2 and +1.5 ‰VPDB. Cc3 has $\delta^{18}\text{O}$ values between -14.3 and -13.4 ‰VPDB and $\delta^{13}\text{C}$ values between -9.3 and -6.9 ‰VPDB. Cc4 exhibits $\delta^{18}\text{O}$ values
265 between -13.8 and -13.4 ‰VPDB and $\delta^{13}\text{C}$ values between -7.4 and -7.2 ‰VPDB and Cc5 ranges in $\delta^{18}\text{O}$ between -8.1 and -5.7 ‰VPDB and in $\delta^{13}\text{C}$ between -8.2 and -3.8 ‰VPDB. The calcite cement Cc1a, precipitated in the fault zone affecting the Devonian hanging wall, has enriched $\delta^{13}\text{C}$ values, whilst the calcite cement within the fault plane (Cc2) exhibits either negative or positive $\delta^{13}\text{C}$ values and the calcite cements hosted in the Stephano-Permian andesites (Cc3 to Cc5) have more depleted $\delta^{13}\text{C}$ values (Fig. 9). In addition, calcite cements show a progressive depletion in $\delta^{18}\text{O}$ from Cc1a to Cc4, whereas Cc5 displays
270 more enriched $\delta^{18}\text{O}$ values.

The obtained Δ_{47} values from clumped isotope thermometry were converted into temperatures and $\delta^{18}\text{O}_{\text{fluid}}$ (Table 1 and Fig. 10) using the equation of Kluge et al., (2015) and Friedman and O'Neil, (1977), respectively. Cc2 has a Δ_{47} of 0.567, which translates into a temperature between 56 and 98 °C and a $\delta^{18}\text{O}_{\text{fluid}}$ between -6.4 and -0.3 ‰VSMOW. For Cc3, Δ_{47} is 0.045 and the calculated T and $\delta^{18}\text{O}_{\text{fluid}}$ are 127 to 208 °C and +4.3 to +12.1 ‰VSMOW, respectively. Δ_{47} for Cc4 is 0.48, which translates
275 into a T and a $\delta^{18}\text{O}_{\text{fluid}}$ between 102 to 167 °C and +0.9 to +8.1 ‰VSMOW, respectively. For Cc5 the Δ_{47} is 0.77 and the calculated T and a $\delta^{18}\text{O}_{\text{fluid}}$ are between -5 and +3 °C and between -12.4 and -10.1 ‰VSMOW, respectively.

The $^{87}\text{Sr}/^{86}\text{Sr}$ ratio of calcite cements Cc1a to Cc5 and host rocks are reported in Table 1 and Fig. 11. Devonian limestones from the hanging wall have a $^{87}\text{Sr}/^{86}\text{Sr}$ ratio of 0.710663, whilst the Stephano-Permian andesites in the footwall exhibit a more radiogenic $^{87}\text{Sr}/^{86}\text{Sr}$ ratio of 0.743983. The calcite cements have more radiogenic $^{87}\text{Sr}/^{86}\text{Sr}$ ratios than the Devonian limestones
280 but less radiogenic values than the Stephano-Permian andesites. This ratio ranges from 0.713018 to 0.714092 in Cc1a, is 0.718294 for Cc2, 0.714619 for Cc3, 0.717706 for Cc4 and 0.716923 for Cc5. These results are compared with already published data from synkinematic veins and deformed rocks in other Pyrenean structures developed in the basement and in the sedimentary cover during the Pyrenean compression (Fig. 11). This comparison shows that values obtained in this study are:
1) significantly more radiogenic than the values of marine carbonates and synkinematic veins precipitated in the sedimentary
285 cover (i.e., in the South Pyrenean fault and thrust belt); and, 2) within the same range of values of synkinematic veins and deformed rocks in the Pyrenean basement (Axial Zone).

The analyzed samples for $^{143}\text{Nd}/^{144}\text{Nd}$ ratios in calcite cements and host rocks are reported in Table 1. However, due to the general low Nd concentrations in most of the analyzed calcite cements and the limited amount of powdered samples that were available, only calcite cement Cc5 and the andesite host rock (footwall) could be measured. Cc5 has a $^{143}\text{Nd}/^{144}\text{Nd}$ ratio of
290 0.512178, which is similar to the one of its footwall host rocks, which is 0.512196.

The obtained elemental composition broadly varies among the different calcite cements and related host rocks (Table 2 and Fig. 12). In the thrust zone affecting the hanging wall, calcite cement Cc1a shows a similar trend to that of the Devonian limestones, both having high Sr, intermediate-high Mg and Fe and low Mn contents (Fig. 12). In the main thrust plane, calcite



295 cement Cc2 has low Mg and Fe and intermediate Mn and Sr contents with respect to the other cements. In the footwall, Cc3 and Cc4 have similar elemental composition, characterized by high Mn, intermediate-high Sr, intermediate-low Fe and low Mg contents. Finally, calcite cement Cc5 follows a similar trend to that of the Stephano-Permian andesites, both having the highest Fe and Mg and the lowest Sr and Mn contents with respect to the other cements and host rocks.

5 Discussion

5.1 Chronology of the observed structures

300 The Estamariu thrust, affecting basement rocks in the Axial Pyrenees, resulted from a long-lived tectonic history that lasted from Variscan to Neogene times. U-Pb dating of calcite cements Cc1a to Cc5 failed due to their high lead contents and low uranium contents and therefore, the timing of the different mesostructures and microstructures has been determined by means of crosscutting relationships and microstructural analysis.

The Paleozoic metasedimentary rocks from the Pyrenean basement are broadly affected by multiscale folds and axial plane regional foliation, developed during the main Variscan deformation phase (Bons, 1988; Cochelin et al., 2018; Zwart, 1986). 305 Similar structures, a decametric-scale anticline and pervasive axial plane foliation, are found in the Devonian sequence located in the thrust hanging wall (Fig. 2B) and therefore, we consider them to be developed during the Variscan compression, contemporaneous with the main activity of the Estamariu thrust. Veins V0 are perpendicular to stylolites e1 and show ambiguous crosscutting relationships between them. Thus, they are interpreted as originated coevally. Both microstructures 310 are concentrated into discontinuous fragments of the Devonian host rocks and are therefore considered inherited microstructures likely developed in Variscan times. However, as pointed above, in the study area the Estamariu thrust affects late- to post-Variscan Stephano-Permian andesites, confirming thus its reactivation during the Alpine orogeny. Accordingly, the structures that are strictly attributed to the Alpine reactivation of the thrust are those structures indicating reverse kinematics or associated with a compressional stress, which are found within the thrust zone deformation, at the contact between Devonian 315 and Stephano-Permian units. Contrarily, the magmatic layering and joints J1 are broadly present in the andesitic footwall, outside the thrust zone, and in other Stephano-Permian basins, and are therefore considered inherited fluidal and cooling structures, respectively. For this reason, the calcite veins V1a and V2 (and related cements Cc1a and Cc2), exclusively occurring within the thrust zone, have been associated with the reactivation of the Estamariu thrust. During this period, and associated with ongoing deformation and progressive shortening, stylolites e2 developed as sutured areas between host rock 320 and veins V1a and between foliation surfaces, coevally with the development of veins V1b, as denoted by their crosscutting relationships and orientations.

Other structures present in the study area, such as veins V3 to V5 and related cements Cc3 to Cc5, are attributed to the Neogene extension. Veins V3 precipitated in the subsidiary thrust zone developed in the footwall of the Estamariu thrust. These veins strike parallel to the thrust zone foliation (Fig 7A, B) but are characterized by calcite fibers growing perpendicular to the vein 325 walls and to the foliation surfaces (Fig. 7C), thus evidencing their extensional character. The presence of extensional calcite



veins opened along previously formed foliation surfaces in a thrust zone has been reported in other structures in the Pyrenees and has been considered to postdate the thrust activity (Lacroix et al., 2011, 2014). Veins V4 precipitated in subvertical and E-W mesoscale faults affecting the Stephano-Permian andesites (Fig. 8), outside the thrust zone (Fig. 3). The fault orientation and dip and the two striae set generations observed on the fault planes are compatible with the Neogene extensional faults that bound the Cerc basin and postdate the Estamariu thrust (Cabrera et al., 1988; Roca, 1996; Saura, 2004). calcite cements Cc3 and Cc4, occluding veins V3 and V4, have a similar geochemical composition (Fig. 9 – 12), supporting that their precipitation occurred during the same tectonic event and associated with a similar fluid regime. Finally, veins V5 (and related cement Cc5) precipitated locally in shear fractures crosscutting and postdating the thrust-related deformation (Fig. 3, 4 and 8D). These veins strike parallel to the shear bands (Cn) located in the main thrust zone (Fig. 8E), exhibiting normal slip kinematics, postdating the reverse structures and therefore indicating reactivation of the Estamariu thrust during the Neogene extension.

5.2 Fluid system during the Alpine reactivation of the Estamariu thrust

As veins V1a and V2 developed during the Alpine reactivation of the Estamariu thrust, the geochemistry of their related calcite cements Cc1a and Cc2 record the fluid system during this tectonic event.

Calcite cements Cc1a and Cc2 are characterized by high $^{87}\text{Sr}/^{86}\text{Sr}$ ratios (from 0.713 to 0.714 for Cc1a and 0.718 for Cc2), significantly more radiogenic than ratios of Phanerozoic seawater (between 0.7070 and 0.7090) (McArthur et al., 2012). This may reflect the incorporation of radiogenic Sr from a fluid derived or interacted with Rb-rich crystalline basement rocks such as those underlying the Estamariu thrust. Previous studies reported similar $^{87}\text{Sr}/^{86}\text{Sr}$ ratios in crystalline rocks and in synkinematic veins developed in the Pyrenean basement (Wayne and McCaig, 1998; McCaig et al., 1995; Banks et al., 1991; Bickle et al., 1988) (Fig. 11). Contrarily, rocks from the Mesozoic-Cenozoic cover in the Southern Pyrenean fold and thrust belt have similar or slightly higher $^{87}\text{Sr}/^{86}\text{Sr}$ ratios with respect to Phanerozoic seawater (Fig. 11). On the other hand, Cc1a has a narrow range of $\delta^{13}\text{C}$, between +0.91 and +2 ‰VPDB, consistent with values of the Devonian marine limestones from the hanging wall (between +1.54 and +2.75 ‰VPDB) and within the range of Devonian marine carbonate values (Veizer et al., 1999). Likewise, the elemental composition of Cc1a follows a trend similar to that of its Devonian host, both having high Mg and Sr and low Mn contents with respect to the other calcite cements (Fig. 12). These geochemical similarities indicate high fluid-rock interaction and buffering of the carbon and elemental composition of the precipitating fluid by the Devonian carbonates (Marshall, 1992). Calcite cement Cc2 has slightly lower $\delta^{13}\text{C}$, lower Mg and Sr and higher Mn contents with respect to both Cc1a and the Devonian host. On the other hand, the temperature and the $\delta^{18}\text{O}$ composition of the vein-forming fluids, calculated from clumped isotope thermometry of Cc2, range between 56 °C and 96 °C and between -6.4 and -0.3 ‰SMOW, respectively. These values are interpreted as the involvement of heated meteoric fluids. These fluids, which probably heated at depth and enriched in radiogenic Sr during their flow through crystalline basement rocks, flowed channelized along the thrust zone (Fig. 13A) due to the enhanced permeability associated with the thrust discontinuity (McCaig et al., 1995; Trincal et al., 2017). As Cc1a and Cc2 precipitated during the same tectonic event but in different structural positions, they likely precipitated from the same fluids, progressively increasing the fluid-rock interaction from the thrust plane (Cc2) towards the



360 hanging wall (Cc1a). Previous studies already reported channelized syntectonic fluid migration along the thrust zone in other structures from the Pyrenean basement, such as the Gavarnie thrust and the related Pic-de-Port-Vieux thrust (McCaig et al., 1995).

5.3 Fluid system during the Neogene extension

Calcite veins V3 to V5 are attributed to the Neogene extension and the geochemistry of their related calcite cements Cc3 to Cc5 characterize the fluid system during this period.

365 Cc3 and Cc4 have considerably high $^{87}\text{Sr}/^{86}\text{Sr}$ ratios (0.714619 and 0.717706, respectively), similar to the ones reported for Cc1a and Cc2 (Fig. 11), indicating interaction with basement rocks. The $\delta^{18}\text{O}_{\text{fluid}}$ calculated from clumped isotopes, between +4.3 and +12.1 ‰SMOW for Cc3 and between +0.9 and +8.1 ‰SMOW for Cc4, falls within the range of metamorphic and/or formation brines (Taylor, 1987). The $\delta^{18}\text{O}$ -depleted values of these cements (around -14 ‰VPDB) are due to the high
370 geothermal gradient of 30 °C, these temperatures would have been reached at a minimum depth of 3 – 5 km. However, these veins have never reached such a burial depth, since during the Neogene extension the studied structure acquired its current configuration (Saura, 2004) and was only buried under the Devonian sequence (hanging wall), which has a maximum thickness of several hundred meters (Mey, 1967). This assumption evidences the hydrothermal character of the circulating fluids. Similarly, the high Mn content of Cc3 and Cc4 (around 7700-8300 and 4000 ppm, respectively), responsible of their bright
375 luminescence (Fig. 7D, 8C), is consistent with hydrothermal waters (Pfeifer et al., 1988; Pomerol, 1983; Pratt et al., 1991). On the other hand, the $\delta^{13}\text{C}$ -depleted values of these cements are indicative of the influence of organic derived carbon (Cerling, 1984; Vilasi et al., 2006). The most probable source for these low $\delta^{13}\text{C}$ values is the Silurian black shales that do not crop out in the study area but acted as the main detachment level during the Variscan compression, and locally during the Alpine compression, in the Pyrenean Axial Zone (Mey, 1967). These black shales have significant organic carbon contents (TOC
380 around 2.3%), and around the Gavarnie thrust, these shales have syntectonic carbonate veins yielding $\delta^{13}\text{C}$ values between -2 and -8 ‰VPDB (McCaig et al., 1995). Thus, cements Cc3 and Cc4 precipitated from hydrothermal fluids derived and/or equilibrated with crystalline basement rocks and expelled through newly formed and reactivated fault zones during deformation (Fig. 13B).

Finally, the isotopic signature of Cc5, ranging between -8.1 and -5.7 ‰VPDB for $\delta^{18}\text{O}$ and between -8.2 and -3.8 ‰VPDB
385 for $\delta^{13}\text{C}$, indicates a meteoric origin. The similar tendency in the elemental composition of this cement and the Stephano-Permian volcanic rocks, both having the highest Mg and Fe and the lowest Mn and Sr contents with respect to the other cements and host rocks, reveals high fluid-rock interaction with the footwall rocks. The significant water-rock interaction is also demonstrated by the Nd isotopic composition of Cc5 (0.512178), yielding to values of the volcanic host (0.512196). This fact, together with the scarcity and small size of Cc5 veins, indicate that this cement precipitated from percolation of meteoric fluids,
390 which geochemistry was controlled by its volcanic host rock. The $\delta^{18}\text{O}_{\text{fluid}}$ and the temperature of precipitation calculated from clumped isotopes, ranging between -12.4 and -10.1 ‰SMOW and between -5 and 3 °C, respectively, corroborate the meteoric



origin and may be indicative of high latitude and/or high altitude conditions (Dansgaard, 1964). During the Neogene, the study area was approximately at the same latitude than today (Smith, 1996). Studies focused on infiltration of meteoric fluids and subsequent upflowing along La Tet fault during the Neogene extension, have shown that meteoric waters in the area infiltrate at high altitudes, around 2000 m, and low temperatures, around 5 °C (Krimissa et al., 1994; Taillefer et al., 2018). On the other hand, the widespread presence of glacial and fluvio-glacial deposits has been reported unconformably overlying the Neogene basin infill and the Variscan rocks from the eastern Axial Pyrenees (Roca, 1996; Turu i Michels and Peña, 2006). These deposits reflect several Quaternary glacial periods in the area, which in turn could have contributed to the low temperature and low $\delta^{18}\text{O}_{\text{fluid}}$ (Gregory et al., 1989). In any case, precipitation of Cc5 probably took place during the latest stages of extension, after the fluid regime changed from upward fluid migration to percolation of cold meteoric waters, as also occurred in the Barcelona Plain (Catalan Coastal Ranges) (Cantarero et al., 2014b).

5.4 Influence of crystalline basement rocks on fluid chemistry during deformation

The aim of this study was to provide insights into the behavior and evolution of fluids circulating through a long-lived thrust, and to determine the influence of basement rocks on the fluid chemistry during deformation. As pointed above, previous studies constrained the relationship between deformation and fluid migration in other structures from the Mesozoic and Cenozoic cover (Muñoz-López et al., under review; Cruset et al., 2016, 2018; Travé et al., 1997, 2000), and to a lesser extent, from the Paleozoic basement (Banks et al., 1991; McCaig et al., 1995, 2000b; Wayne and McCaig, 1998). The comparison between these studies and the new data provided in this contribution evidences that fluids migrating through basement or cover units have a different geochemical signature. This signature is recorded in the vein cements, particularly in their $^{87}\text{Sr}/^{86}\text{Sr}$ ratios. Accordingly, the high $^{87}\text{Sr}/^{86}\text{Sr}$ ratios (0.713 to 0.718) of the analyzed calcite cements, originated during successive compressional and extensional tectonic events, indicate that regardless of the origin of the fluids and the tectonic context, basement rocks have a significant influence on the fluid chemistry. This means that cements precipitated from fluids that have circulated through crystalline basement rocks have significantly high $^{87}\text{Sr}/^{86}\text{Sr}$ ratios (> 0.710) (Fig. 11), reflecting the interaction between the vein-forming fluids with Rb-rich source rocks. Similar high radiogenic $^{87}\text{Sr}/^{86}\text{Sr}$ ratios have also been attributed to basement-derived fluids in the Glarus nappe (Swiss Alps) (Burkhard et al., 1992). By contrast, vein cements precipitated from fluids that have circulated through the Mesozoic-Cenozoic sedimentary cover in the Pyrenees have significantly lower $^{87}\text{Sr}/^{86}\text{Sr}$ ratios (< 0.710). Such lower values may be similar to Phanerozoic seawater values, evidencing interaction between the vein-forming fluids and marine carbonate units, or higher, evidencing interaction with siliciclastic rocks (Cruset et al., 2018; Travé et al., 2007). A previous study, focused on fluid flow along the Gavarnie thrust in the central-western Axial Pyrenees, used this limit value ($^{87}\text{Sr}/^{86}\text{Sr} = 0.710$) to differentiate between the unaltered limestone protolith and the Cretaceous thrust-related carbonate mylonite affected by fluids carrying radiogenic Sr (McCaig et al., 1995).



5.5 Fluid flow at regional scale: the NE part of the Iberian Peninsula during the Neogene extension

During the late Oligocene to middle Miocene, the opening of the NW Mediterranean Sea was responsible for the development of a complex ENE-WSW to NE-SW extensional fault system in the NE part of the Iberian Peninsula (Roca, 1996; Roca and Guimerà, 1992; Vergés et al., 2002). In the eastern Axial Pyrenees, La Tet fault is the main Neogene structure and has associated major E-W extensional faults, such as the Ortedó and La Seu d'Urgell faults, which crosscut the Alpine structures (e.g., the reactivation of the Estamariu thrust) and delimitate the Cerc basin (Fig. 1). Within this basin, E-W mesoscale normal faults (veins V4) also developed during this period and previously formed weakness surfaces were reopened (i.e., the thrust zone foliation associated with the Estamariu thrust, veins V3). During this episode, calcite cements Cc3 and Cc4 precipitated from hydrothermal fluids (temperatures between 102 and 208 °C) derived and/or interacted at depth with crystalline basement rocks before ascending through newly formed fault zones and reactivated structures. These interpretations are consistent with the presence of several hydrothermal springs (temperatures of 29 °C to 73 °C) currently upwelling aligned along La Tet fault and related Neogene deformation in the Pyrenean Axial Zone (Krimissa et al., 1994; Taillefer et al., 2017, 2018). Several studies indicate the origin of these hot water springs as meteoric fluids, infiltrated at high-elevated reliefs, above 2000 m, warmed at great depths by normal geothermal gradients, and migrated upwards along permeability anisotropies related to fault zones (Taillefer et al., 2017, 2018). The geochemical analysis of these springs, and in particular their high radiogenic $^{87}\text{Sr}/^{86}\text{Sr}$ ratios, ranging between 0.715 and 0.730, according to French Geological Survey reports (Caballero et al., 2012), are within the range of values obtained in this study and also accounts for interaction between circulating fluids and crystalline basement rocks. Studies based on numerical models suggest that La Tet fault and the involved crystalline rocks are still permeable down to 3 km depth (Taillefer et al., 2017, 2018), although the fault has been dormant since the Mio-Pliocene (Goula et al., 1999). These authors also suggest that the footwall topography is the major factor controlling the infiltration of meteoric fluids and the recharge of the hydrothermal system. The topography, which induces high hydraulic gradients and produces fluid advection, controls the circulation depth and therefore, the maximum temperature reached by the migrating fluids (Taillefer et al., 2017).

A similar geological context and fluid regime evolution to that explained above is found in the Barcelona Plain and the Vallès Basin, located in the northeast part of the Catalan Coastal Ranges (CCR) (Fig. 1A). Consequently, the comparison between both geological contexts allows us to give insights into the fluid circulation in extensional basins at regional scale (in the NE part of Iberia). In these locations of the CCR, the main fault system associated with the Neogene extension acted as conduits for hydrothermal fluid circulation at temperatures between 130 and 150 °C during synkinematic periods (Cantarero et al., 2014a, 2014b; Cardellach et al., 2002), and is also responsible for the present-day circulation of hot water springs up to 70 °C (Carmona et al., 2000; Fernández and Banda, 1990). In both cases, fluids would have been topographically driven from elevated areas to great depths (Cantarero et al., 2014b), where they circulated through crystalline rocks, acquiring high $^{87}\text{Sr}/^{86}\text{Sr}$ ratios (> 0.712) and high temperatures (Cardellach et al., 2002) before ascending through fault discontinuities. However, in the Penedès basin, which corresponds to the southwestern termination of the Neogene structure in the CCR, crystalline



455 basement rocks do not crop out and the extensional faults only involve Neogene deposits filling the basin and a Mesozoic
sedimentary substrate. In this location, the main fault system acted as conduits for several episodes of meteoric fluids
percolation during the Neogene extension and evidence of hydrothermal fluid circulation has not been reported in the area
(Travé and Calvet, 2001; Travé et al., 1998; Baqués et al., 2012, 2010). This fact agrees with previous studies that highlight
that hydrothermal activity, and in particular the occurrence of hot water springs in the Pyrenees and in the CCR, is preferably
460 concentrated in basement rocks, which constitute the elevated footwall of the main extensional fault systems (Taillefer et al.,
2017; Carmona et al., 2000).

All these observations indicate that the fluids responsible for precipitation of synkinematic cements during Neogene times in
the eastern Axial Pyrenees and in the northeast part of the CCR, and fluids currently flowing through Neogene extensional
faults in both places are hydrothermal and have crystalline basement rocks as a common reservoir. This evidences an open
465 fluid system in the NE part of the Iberian Peninsula associated with the Neogene extensional deformation. Accordingly, this
extensional fault system has acted as a conduit for long-term circulation of hot fluids from Neogene times to present. This
long-term fault-controlled fluid flow could have been continuous through time or could be related to intermittent pulses. Fault
control on upflowing of hot fluids along fault systems is a common process in different geological settings and has been
reported in the Great Basin, USA (Faulds et al., 2010), in the Western Turkey (Faulds et al., 2010), in the Southern Canadian
470 Cordillera (Grasby and Hutcheon, 2001), in the Basin and Range Province (Nelson et al., 2006) and in the southern Tuscany,
Italy (Liotta et al., 2010).

6 Conclusions

The Estamariu thrust, in the Pyrenean Axial Zone, resulted from a multistage Variscan to Neogene tectonic evolution. Our
data, combining structural and petrological observations with geochemical analyses of synkinematic calcite veins and host
475 rocks, provide a structural and diagenetic framework that constrains the fault-fluid system evolution and assesses the
relationships between deformation and fluid migration in the Pyrenean basement. In the study area, the Variscan Estamariu
thrust places a Devonian pre-Variscan unit against a Stephano-Permian late to post-Variscan sequence and therefore, the
structures present within the thrust zone, affecting both sequences, are attributed to the Alpine and subsequent Neogene
reactivation of the thrust. During the Alpine compression, the reactivation of the thrust resulted in the transposition of the
480 Variscan regional foliation within the thrust zone and in the formation of a subsidiary thrust zone affecting the andesites in the
footwall. During this period, meteoric fluids interacted with the crystalline basement and migrated upwards along the thrust
and related structures at temperatures between 56 and 98 °C. These fluids progressively increased the fluid-rock interaction
from the thrust plane towards the hanging wall. During the Neogene extension, the Estamariu thrust was reactivated and normal
faults and shear fractures were formed. These structures allowed basement-derived fluids to flow upwards through reactivated
485 and newly formed fault zones at temperatures up to 208 °C. Finally, during the latest to post stages of extension and uplift of



the structure, the fluid regime changed to percolation of low temperature meteoric fluids that were buffered by the volcanic host rocks.

The comparison between our results and previously published data allows us to provide insights into the fluid characteristics and fluid regime at regional scale. On the one hand, the influence of basement rocks on the fluid chemistry during deformation in the Pyrenees has been assessed. In this sense, regardless the fluid origin and the tectonic context, the fluids that have interacted with crystalline basement rocks have a significantly higher $^{87}\text{Sr}/^{86}\text{Sr}$ ratio (> 0.710) with respect to those that have circulated through the sedimentary cover (< 0.710). On the other hand, a similar fluid regime associated with the Neogene extension in the NE part of the Iberian Peninsula (including the eastern Pyrenees and the northeastern part of the Catalan Coastal Ranges) has been observed. In both settings, the extensional deformation structures have acted as conduits for long-term fluid migration from Neogene times to present. Migrating fluids during this period are hydrothermal and have interacted with crystalline rocks before ascending through fault zones and related structures.

Acknowledgments

Carbon and oxygen isotopic analyses were carried out at “Centre Científics i Tecnològics” of the Universitat de Barcelona. Strontium and Neodymium analyses were performed at the “CAI de Geocronología y Geoquímica Isotópica” of the Universidad Complutense de Madrid. The Elemental composition was analysed at the Geochemistry Facility of labGEOTOP of the Institute of Earth Sciences Jaume Almera (ICTJA-CSIC). Clumped isotope thermometry was carried out at the Imperial College London. This research was carried out within the framework of DGICYT Spanish Project PGC2018-093903-B-C22 (Ministerio de Ciencia, Innovación y Universidades / Agencia Estatal de Investigación / Fondo Europeo de Desarrollo Regional, Unión Europea) and the Grup Consolidat de Recerca “Geologia Sedimentària” (2017-SGR- 824). The PhD research of DM-L is supported by the FPI2016 (BES-2016-077214) Spanish program from MINECO.

References

- Banks, D., Da Vies, G., Yardley, B. W., McCaig, A. and Grant, N.: The chemistry of brines from an Alpine thrust system in the Central Pyrenees: An application of fluid inclusion analysis to the study of fluid behaviour in orogenesis, *Geochim. Cosmochim. Acta*, 55(4), 1021–1030, doi:10.1016/0016-7037(91)90160-7, 1991.
- Baqués, V., Travé, A., Benedicto, A., Labaume, P., Cantarero, I.: Relationships between carbonate fault rocks and fluid flow regime during propagation of the Neogene extensional fault of the Penedès basin (Catalan Coastal Ranges, NE Spain), *Journal of Geochemical Exploration*, 106, 24–33, 2010.
- Baqués, V., Travé, A., Roca, E., Marin, M. and Cantarero, I.: Geofluid behaviour in successive extensional and compressional events: a case study from the southwestern end of the Valles-Penedes Fault (Catalan Coastal Ranges, NE Spain), *Pet. Geosci.*, 18(1), 17–31, doi:10.1144/1354-079311-017, 2012.



- Barker, S. L. L., Bennett, V. C., Cox, S. F., Norman, M. D. and Gagan, M. K.: Sm–Nd, Sr, C and O isotope systematics in hydrothermal calcite–fluorite veins: Implications for fluid–rock reaction and geochronology, *Chem. Geol.*, 268(1–2), 58–66, doi:10.1016/j.chemgeo.2009.07.009, 2009.
- Beaudoin, N., Bellahsen, N., Lacombe, O., Emmanuel, L. and Pironon, J.: Crustal-scale fluid flow during the tectonic evolution of the Bighorn Basin (Wyoming, USA), *Basin Res.*, 26(3), 403–435, doi:10.1111/bre.12032, 2014.
- 520 Beaudoin, N., Huyghe, D., Bellahsen, N., Lacombe, O., Emmanuel, L., Mouthereau, F. and Ouahnon, L.: Fluid systems and fracture development during syn-depositional fold growth: An example from the Pico del Aguila anticline, Sierras Exteriores, southern Pyrenees, Spain, *J. Struct. Geol.*, 70, 23–38, doi:10.1016/j.jsg.2014.11.003, 2015.
- Bickle, M. J., Wickham, S. M., Chapman, H. J. and Taylor, H. P.: A strontium, neodymium and oxygen isotope study of hydrothermal metamorphism and crustal anatexis in the Trois Seigneurs Massif, Pyrenees, France, *Contrib. to Mineral. Petrol.*, 100(4), 399–417, doi:10.1007/BF00371371, 1988.
- 525 Bons, A.: Intracrystalline deformation and slaty cleavage development in very low-grade slates from the Central Pyrenees, *Geol. Ultraiectina*, 1988.
- Breesch, L., Swennen, R. and Vincent, B.: Fluid flow reconstruction in hanging and footwall carbonates: Compartmentalization by Cenozoic reverse faulting in the Northern Oman Mountains (UAE), *Mar. Pet. Geol.*, 26(1), 113–128, doi:10.1016/j.marpetgeo.2007.10.004, 2009.
- 530 Burkhard, M., Kerrich, R., Maas, R. and Fyfe, W. S.: Stable and Sr-isotope evidence for fluid advection during thrusting of the glarus nappe (Swiss Alps), *Contrib. to Mineral. Petrol.*, 112(2–3), 293–311, doi:10.1007/BF00310462, 1992.
- Caballero, Y., Gironde, C. and Le Goff, E.: Ressource en eau thermale de la station d’Amélie-les-Bains. Etat des lieux. Rapport BRGM/RP-60618-FR., 2012.
- 535 Cabrera, L., Roca, E. and Santanach, P.: Basin formation at the end of a strike-slip fault: the Cerdanya Basin (eastern Pyrenees), *J. Geol. Soc. London.*, 145(2), 261–268, doi:10.1144/gsjgs.145.2.0261, 1988.
- Cantarero, I., Lanari, P., Vidal, O., Alías, G., Travé, A., Baqués, V.: Long-term fluid circulation in extensional faults in the Central Catalan Coastal Ranges: P-T constraints from neofomed chlorite and K-white mica, *Int. J. Earth Sci.* 03, 165–188, 2014a.
- 540 Cantarero, I., Travé, A., Alías, G. and Baqués, V.: Polyphasic hydrothermal and meteoric fluid regimes during the growth of a segmented fault involving crystalline and carbonate rocks (Barcelona Plain, NE Spain), *Geofluids*, 14(1), 20–44, doi:10.1111/gfl.12021, 2014b.
- Cardellach, E., Canals, À. and Grandia, F.: Recurrent hydrothermal activity induced by successive extensional episodes: the case of the Berta F–(Pb–Zn) vein system (NE Spain), *Ore Geol. Rev.*, 22(1–2), 133–141, doi:10.1016/S0169-1368(02)00112-9, 2002.
- 545 Carmona, J. M., Bitzer, K., López, E. and Bouazza, M.: Isotopic composition and origin of geothermal waters at Caldetes (Maresme-Barcelona), *J. Geochemical Explor.*, 69–70, 441–447, doi:10.1016/S0375-6742(00)00127-8, 2000.
- Cerling, T. E.: The stable isotopic composition of modern soil carbonate and its relationship to climate, *Earth Planet. Sci. Lett.*,



- 550 doi:10.1016/0012-821X(84)90089-X, 1984.
- Choukroune, P.: The Ecore Pyrenean deep seismic profile reflection data and the overall structure of an orogenic belt, *Tectonics*, doi:10.1029/TC008i001p00023, 1989.
- Cochelin, B., Lemirre, B., Denèle, Y., de Saint Blanquat, M., Lahfid, A. and Duchêne, S.: Structural inheritance in the Central Pyrenees: the Variscan to Alpine tectonometamorphic evolution of the Axial Zone, *J. Geol. Soc. London.*, 175(2), 336–351,
555 doi:10.1144/jgs2017-066, 2018.
- Cox, S. F.: Structural and isotopic constraints on fluid flow regimes and fluid pathways during upper crustal deformation: An example from the Taemas area of the Lachlan Orogen, SE Australia, *J. Geophys. Res.*, 112(B8), B08208, doi:10.1029/2006JB004734, 2007.
- Crespo-Blanc, A., Masson, H., Sharp, Z., Cosca, M. and Hunziker, J.: A stable and $^{40}\text{Ar}/^{39}\text{Ar}$ isotope study of a major thrust
560 in the Helvetic nappes (Swiss Alps): Evidence for fluid flow and constraints on nappe kinematics, *Geol. Soc. Am. Bull.*, 107(10), 1129–1144, doi:10.1130/0016-7606(1995)107<1129:ASAAAI>2.3.CO;2, 1995.
- Crognier, N., Hoareau, G., Aubourg, C., Dubois, M., Lacroix, B., Branellec, M., Callot, J. P. and Vennemann, T.: Syn-orogenic fluid flow in the Jaca basin (south Pyrenean fold and thrust belt) from fracture and vein analyses, *Basin Res.*, 30(2), 187–216, doi:10.1111/bre.12249, 2018.
- 565 Cruset, D.: Sequential fluid migration along a fold and thrust belt SE pyrenees from late Cretaceous to Oligocene, PhD thesis, Universitat de Barcelona., 2019.
- Cruset, D., Cantarero, I., Travé, A., Vergés, J. and John, C. M.: Crestal graben fluid evolution during growth of the Puig-reig anticline (South Pyrenean fold and thrust belt), *J. Geodyn.*, 101, 30–50, doi:10.1016/j.jog.2016.05.004, 2016.
- Cruset, D., Cantarero, I., Vergés, J., John, C. M., Muñoz-López, D. and Travé, A.: Changes in fluid regime in syn-orogenic
570 sediments during the growth of the south Pyrenean fold and thrust belt, *Glob. Planet. Change*, 171(October 2017), 207–224, doi:10.1016/j.gloplacha.2017.11.001, 2018.
- Dansgaard, W.: Stable isotopes in precipitation, *Tellus*, doi:10.3402/tellusa.v16i4.8993, 1964.
- Dennis, K. J., Affek, H. P., Passey, B. H., Schrag, D. P. and Eiler, J. M.: Defining an absolute reference frame for ‘clumped’ isotope studies of CO_2 , *Geochim. Cosmochim. Acta*, 75(22), 7117–7131, doi:10.1016/j.gca.2011.09.025, 2011.
- 575 Dewever, B., Swennen, R. and Breesch, L.: Fluid flow compartmentalization in the Sicilian fold and thrust belt: Implications for the regional aqueous fluid flow and oil migration history, *Tectonophysics*, 591, 194–209, doi:10.1016/j.tecto.2011.08.009, 2013.
- Faulds, J., Coolbaugh, M., Bouchot, V., Moeck, I., Oğuz, K. and Cedex, O.: Characterizing Structural Controls of Geothermal Reservoirs in the Great Basin , USA , and Western Turkey : Developing Successful Exploration Strategies in Extended
580 Terranes, *World, C*(2010), 25–29, 2010.
- Faj-Gomord, O., Allanic, C., Verbiest, M., Honlet, R., Champenois, F., Bonifacie, M., Chaduteau, C., Wouters, S., Muchez, P., Lasseur, E. and Swennen, R.: Understanding Fluid Flow during Tectonic Reactivation: An Example from the Flamborough Head Chalk Outcrop (UK), *Geofluids*, 2018, 1–17, doi:10.1155/2018/9352143, 2018.



- Fernàndez, M. and Banda, E.: Geothermal anomalies in the Valles-Penedes Graben Master Fault: Convection through the
585 Horst as a possible mechanism, *J. Geophys. Res.*, 95(B4), 4887, doi:10.1029/JB095iB04p04887, 1990.
- Fitz-Diaz, E., Hudleston, P., Siebenaller, L., Kirschner, D., Camprubí, A., Tolson, G. and Puig, T. P.: Insights into fluid flow
and water-rock interaction during deformation of carbonate sequences in the Mexican fold-thrust belt, *J. Struct. Geol.*, 33(8),
1237–1253, doi:10.1016/j.jsg.2011.05.009, 2011.
- Foden, J.: Sr-isotopic evidence for Late Neoproterozoic rifting in the Adelaide Geosyncline at 586 Ma: implications for a Cu
590 ore forming fluid flux, *Precambrian Res.*, 106(3–4), 291–308, doi:10.1016/S0301-9268(00)00132-7, 2001.
- Fontana, S., Nader, F. H., Morad, S., Ceriani, A., Al-Aasm, I. S., Daniel, J. M. and Mengus, J. M.: Fluid-rock interactions
associated with regional tectonics and basin evolution, *Sedimentology*, 61(3), 660–690, doi:10.1111/sed.12073, 2014.
- Friedman, I. and O’Neil, J. R.: Compilation of stable isotope fractionation factors of geochemical interest, in *Professional
Papers.*, 1977.
- 595 García-Sansegundo, J., Poblet, J., Alonso, J. L. and Clariana, P.: Hinterland-foreland zonation of the Variscan orogen in the
Central Pyrenees: comparison with the northern part of the Iberian Variscan Massif, *Geol. Soc. London, Spec. Publ.*, 349(1),
169–184, doi:10.1144/SP349.9, 2011.
- Gasparrini, M., Ruggieri, G. and Brogi, A.: Diagenesis versus hydrothermalism and fluid-rock interaction within the Tuscan
Nappe of the Monte Amiata CO₂ -rich geothermal area (Italy), *Geofluids*, 13(2), 159–179, doi:10.1111/gfl.12025, 2013.
- 600 Gomez-Rivas, E., Bons, P. D., Koehn, D., Urai, J. L., Arndt, M., Virgo, S., Laurich, B., Zeeb, C., Stark, L. and Blum, P.: The
Jabal Akhdar dome in the Oman Mountains: Evolution of a dynamic fracture system, *Am. J. Sci.*, 314(7), 1104–1139,
doi:10.2475/07.2014.02, 2014.
- Goula, X., Olivera, C., Fleta, J., Grellet, B., Lindo, R., Rivera, L. A., Cisternas, A. and Carbon, D.: Present and recent stress
regime in the eastern part of the Pyrenees, *Tectonophysics*, doi:10.1016/S0040-1951(99)00120-1, 1999.
- 605 Grant, N. T., Banks, D. A., McCaig, A. M. and Yardley, B. W. D.: Chemistry, source, and behavior of fluids involved in alpine
thrusting of the Central Pyrenees, *J. Geophys. Res.*, 95(B6), 9123, doi:10.1029/JB095iB06p09123, 1990.
- Grasby, S. E. and Hutcheon, I.: Controls on the distribution of thermal springs in the southern Canadian Cordillera, *Can. J.
Earth Sci.*, 38(3), 427–440, doi:10.1139/cjes-38-3-427, 2001.
- Gregory, R. T., Douthitt, C. B., Duddy, I. R., Rich, P. V. and Rich, T. H.: Oxygen isotopic composition of carbonate concretions
610 from the lower Cretaceous of Victoria, Australia: implications for the evolution of meteoric waters on the Australian continent
in a paleopolar environment, *Earth Planet. Sci. Lett.*, 92(1), 27–42, doi:10.1016/0012-821X(89)90018-6, 1989.
- Guo, W., Mosenfelder, J. L., Goddard, W. A. and Eiler, J. M.: Isotopic fractionations associated with phosphoric acid digestion
of carbonate minerals: Insights from first-principles theoretical modeling and clumped isotope measurements, *Geochim.
Cosmochim. Acta*, 73(24), 7203–7225, doi:10.1016/j.gca.2009.05.071, 2009.
- 615 Hartevelt, J. J. A.: Geology of the Upper Segre and Valira Valleys, Central Pyrenees, Andorra, Spain, Geological Institute,
Leiden University, Leiden : [online] Available from: http://catalog.ub.edu/record=b1043758~S1*cat (Accessed 15 February
2019), 1970.



- Henderson, I. H. C. and McCaig, A. M.: Fluid pressure and salinity variations in shear zone-related veins, central Pyrenees, France: Implications for the fault-valve model, *Tectonophysics*, 262(1–4), 321–348, doi:10.1016/0040-1951(96)00018-2, 1996.
- Huntington, K. W., Eiler, J. M., Affek, H. P., Guo, W., Bonifacie, M., Yeung, L. Y., Thiagarajan, N., Passey, B., Tripathi, A., Daëron, M. and Came, R.: Methods and limitations of “clumped” CO₂ isotope (Δ_{47}) analysis by gas-source isotope ratiomass spectrometry, *J. Mass Spectrom.*, 44(9), 1318–1329, doi:10.1002/jms.1614, 2009.
- John, C. M. and Bowen, D.: Community software for challenging isotope analysis: First applications of ‘Easotope’ to clumped isotopes, *Rapid Commun. Mass Spectrom.*, 30(21), 2285–2300, doi:10.1002/rcm.7720, 2016.
- Kim, S.-T. and O’Neil, J. R.: Equilibrium and nonequilibrium oxygen isotope effects in synthetic carbonates, *Geochim. Cosmochim. Acta*, 61(16), 3461–3475, doi:10.1016/S0016-7037(97)00169-5, 1997.
- Kluge, T., John, C. M., Jourdan, A.-L., Davis, S. and Crawshaw, J.: Laboratory calibration of the calcium carbonate clumped isotope thermometer in the 25–250 °C temperature range, *Geochim. Cosmochim. Acta*, 157, 213–227, doi:10.1016/j.gca.2015.02.028, 2015.
- Krimissa, M., Chery, L., Fouillac, C. and Michelot, J. L.: Origin and Recharge Altitude of the Thermo-Mineral Waters of the Eastern Pyrenees, *Isot. Environ. Heal. Stud.*, 30(4), 317–331, doi:10.1080/00211919408046747, 1994.
- Lacroix, B., Buatier, M., Labaume, P., Travé, A., Dubois, M., Charpentier, D., Ventalon, S. and Convert-Gaubier, D.: Microtectonic and geochemical characterization of thrusting in a foreland basin: Example of the South-Pyrenean orogenic wedge (Spain), *J. Struct. Geol.*, 33(9), 1359–1377, doi:10.1016/j.jsg.2011.06.006, 2011.
- Lacroix, B., Travé, A., Buatier, M., Labaume, P., Vennemann, T. and Dubois, M.: Syntectonic fluid-flow along thrust faults: Example of the South-Pyrenean fold-and-thrust belt, *Mar. Pet. Geol.*, 49, 84–98, doi:10.1016/j.marpetgeo.2013.09.005, 2014.
- Lago, M., Arranz, E., Pocoví, A., Galé, C. and Gil-Imaz, A.: Permian magmatism and basin dynamics in the southern Pyrenees: a record of the transition from late Variscan transtension to early Alpine extension, *Geol. Soc. London, Spec. Publ.*, 223(1), 439–464, doi:10.1144/GSL.SP.2004.223.01.19, 2004.
- Liotta, D., Ruggieri, G., Brogi, A., Fulignati, P., Dini, A. and Nardini, I.: Migration of geothermal fluids in extensional terrains: the ore deposits of the Boccheggiano-Montieri area (southern Tuscany, Italy), *Int. J. Earth Sci.*, 99(3), 623–644, doi:10.1007/s00531-008-0411-3, 2010.
- Marshall, J. D.: Climatic and oceanographic isotopic signals from the carbonate rock record and their preservation, *Geol. Mag.*, doi:10.1017/S0016756800008244, 1992.
- Martí, J.: Genesis of crystal-rich volcanoclastic facies in the Permian red beds of the Central Pyrenees (NE Spain), *Sediment. Geol.*, 106(1–2), 1–19, doi:10.1016/0037-0738(95)00143-3, 1996.
- Martín-Martín, J. D., Travé, A., Gomez-Rivas, E., Salas, R., Sizun, J. P., Vergés, J., Corbella, M., Stafford, S. L. and Alfonso, P.: Fault-controlled and stratabound dolostones in the Late Aptian-earliest Albian Benassal Formation (Maestrat Basin, E Spain): Petrology and geochemistry constrains, *Mar. Pet. Geol.*, 65, doi:10.1016/j.marpetgeo.2015.03.019, 2015.
- Matte, P.: Accretionary history and crustal evolution of the Variscan belt in Western Europe, *Tectonophysics*,



- doi:10.1016/0040-1951(91)90328-P, 1991.
- McArthur, J. M., Howarth, R. J. and Shields, G. A.: Strontium Isotope Stratigraphy, in *The Geologic Time Scale*, vol. 1–2, pp. 127–144, Elsevier., 2012.
- 655 McCaig, A. ., Tritlla, J. and Banks, D.: Fluid mixing and recycling during Pyrenean thrusting: evidence from fluid inclusion halogen ratios, *Geochim. Cosmochim. Acta*, 64(19), 3395–3412, doi:10.1016/S0016-7037(00)00437-3, 2000a.
- McCaig, A. M., Wayne, D. M., Marshall, J. D., Banks, D. and Henderson, I.: Isotopic and fluid inclusion studies of fluid movement along the Gavarnie Thrust, central Pyrenees; reaction fronts in carbonate mylonites, *Am. J. Sci.*, 295(3), 309–343, doi:10.2475/ajs.295.3.309, 1995.
- 660 McCaig, A. M., Wayne, D. M. and Rosenbaum, J. M.: Fluid expulsion and dilatancy pumping during thrusting in the Pyrenees: Pb and Sr isotope evidence, *Geol. Soc. Am. Bull.*, 112(8), 1199–1208, doi:10.1130/0016-7606(2000)112<1199:FEADPD>2.0.CO;2, 2000b.
- McCrea, J. M.: On the isotopic chemistry of carbonates and a paleotemperature scale, *J. Chem. Phys.*, doi:10.1063/1.1747785, 1950.
- 665 Mey, P. H. W.: The geology of the upper Ribagorzana and Baliera Valleys, Central Pyrenees, Spain, *Leidse Geol. Meded.*, 41, 153–220, 1967.
- Mey, P. H. W., Nagtegaal, P. J. C., Roberti, K. J. and Hartevelt, J. J. A.: Lithostratigraphic subdivision of Post-Hercynian deposits in the South-Central Pyrenees, Spain, *Leidse Geol. Meded.*, 41(1), 221–228, 1968.
- Mozafari, M., Swennen, R., Balsamo, F., El Desouky, H., Storti, F. and Taberner, C.: Fault-controlled dolomitization in the
- 670 Montagna dei Fiori Anticline (Central Apennines, Italy): record of a dominantly pre-orogenic fluid migration, *Solid Earth*, 10(4), 1355–1383, doi:10.5194/se-10-1355-2019, 2019.
- Muñoz, J. A.: Evolution of a continental collision belt: ECORS-Pyrenees crustal balanced cross-section, in *Thrust Tectonics*, edited by K. R. McClay, pp. 235–246, Springer Netherlands, Dordrecht., 1992.
- Muñoz, J. A.: Fault-related folds in the southern Pyrenees, *Am. Assoc. Pet. Geol. Bull.*, 101(04), 579–587,
- 675 doi:10.1306/011817DIG17037, 2017.
- Muñoz, J. A., Martinez, A. and Verges, J.: Thrust sequences in the eastern Spanish Pyrenees, *J. Struct. Geol.*, 8, 399–405, 1986.
- Muñoz-López, D., Cruset, D., Cantarero, I., Benedicto, A., Jonh, C. and Travé, A.: Fluid dynamics around a thrust fault inferred from petrology and geochemistry of calcite veins. An example from the southern Pyrenees, *Geofluids*, under review.
- 680 Nardini, N., Muñoz-López, D., Cruset, D., Cantarero, I., Martín-Martín, J., Benedicto, A., Gomez-Rivas, E., John, C. and Travé, A.: From Early Contraction to Post-Folding Fluid Evolution in the Frontal Part of the Bóixols Thrust Sheet (Southern Pyrenees) as Revealed by the Texture and Geochemistry of Calcite Cements, *Minerals*, 9(2), 117, doi:10.3390/min9020117, 2019.
- Nelson, S. T., Mayo, A. L., Gilfillan, S., Dutson, S. J., Harris, R. A., Shipton, Z. K. and Tingey, D. G.: Enhanced fracture
- 685 permeability and accompanying fluid flow in the footwall of a normal fault: The Hurricane fault at Pah Tempe hot springs,



- Washington County, Utah, *Geol. Soc. Am. Bull.*, preprint(2008), 1, doi:10.1130/B26285.1, 2006.
- Pfeifer, H.-R., Oberhänsli, H. and Epprecht, W.: Geochemical evidence for a synsedimentary hydrothermal origin of Jurassic iron-manganese deposits at Gonzen (Sargans, Helvetic Alps, Switzerland), *Mar. Geol.*, 84(3–4), 257–272, doi:10.1016/0025-3227(88)90105-3, 1988.
- 690 Piessens, K., Muchez, P., Dewaele, S., Boyce, A., De Vos, W., Sintubin, M., Debacker, T. N., Burke, E. A. J. and Viaene, W.: Fluid flow, alteration and polysulphide mineralisation associated with a low-angle reverse shear zone in the Lower Palaeozoic of the Anglo-Brabant fold belt, Belgium, *Tectonophysics*, doi:10.1016/S0040-1951(01)00250-5, 2002.
- Poblet, J.: Estructura herciniana i alpina del vessant sud de la zona axial del Pirineu central, Universitat de Barcelona., 1991.
- Pomerol, B.: Geochemistry of the late Cenomanian-early Turonian chalks of the Paris Basin: Manganese and carbon isotopes
695 in carbonates as paleoceanographic indicators, *Cretac. Res.*, 4(1), 85–93, doi:10.1016/0195-6671(83)90025-3, 1983.
- Pratt, L. M., Force, E. R. and Pomerol, B.: Coupled manganese and carbon-isotopic events in marine carbonates at the Cenomanian-Turonian boundary, *J. Sediment. Petrol.*, doi:10.1306/D4267717-2B26-11D7-8648000102C1865D, 1991.
- Roca, E.: The Neogene Cerdanya and Seu d’Urgell intramontane basins (Eastern Pyrenees), in *Tertiary basins of Spain*, edited by P. F. Friend and C. J. Dabrio, pp. 114–119, Cambridge University Press, Cambridge., 1996.
- 700 Roca, E. and Guimerà, J.: The Neogene structure of the eastern Iberian margin: Structural constraints on the crustal evolution of the Valencia trough (western Mediterranean), *Tectonophysics*, 203(1–4), 203–218, doi:10.1016/0040-1951(92)90224-T, 1992.
- Roure, F., Choukroune, P., Berastegui, X., Munoz, J. a., Villien, a., Matheron, P., Bareyt, M., Seguret, M., Camara, P. and Deramond, J.: EORS deep seismic data and balanced cross sections: Geometric constraints on the evolution of the Pyrenees,
705 *Tectonics*, doi:10.1029/TC008i001p00041, 1989.
- Rowland, J. V. and Sibson, R. H.: Structural controls on hydrothermal flow in a segmented rift system, Taupo Volcanic Zone, New Zealand, *Geofluids*, 4(4), 259–283, doi:10.1111/j.1468-8123.2004.00091.x, 2004.
- Rye, D. M. and Bradbury, H. J.: Fluid flow in the crust; an example from a Pyrenean thrust ramp, *Am. J. Sci.*, 288(3), 197–235, doi:10.2475/ajs.288.3.197, 1988.
- 710 Saura, E.: Anàlisi estructural de la Zona de les Nogures (Pirineus Centrals), Universitat de Barcelona., 2004.
- Saura, E. and Teixell, A.: Inversion of small basins: effects on structural variations at the leading edge of the Axial Zone antiformal stack (Southern Pyrenees, Spain), *J. Struct. Geol.*, 28(11), 1909–1920, doi:10.1016/j.jsg.2006.06.005, 2006.
- Sibson, R. H.: Selective fault reactivation during basin inversion: potential for fluid redistribution through fault-valve action, *Geol. Soc. London, Spec. Publ.*, 88(1), 3–19, doi:10.1144/GSL.SP.1995.088.01.02, 1995.
- 715 Sibuet, J. C., Srivastava, S. P. and Spakman, W.: Pyrenean orogeny and plate kinematics, *J. Geophys. Res. B Solid Earth*, 109(8), 1–18, doi:10.1029/2003JB002514, 2004.
- Smith, A. G.: Cenozoic latitudes, positions and topography of the Iberian Peninsula. In: *Tertiary Basins of Spain: The Stratigraphic Record of Crustal Kinematics*. *World and Regional Geology 6* (eds Friend PF, Dabrio CJ), pp. 6–8. Cambridge University Press, Cambridge, 1996.



- 720 Suess E (1979) Mineral phases form
Srivastava, S. P., Schouten, H., Roest, W. R., Klitgord, K. D., Kovacs, L. C., Verhoef, J. and Macnab, R.: Iberian plate kinematics: A jumping plate boundary between Eurasia and Africa, *Nature*, doi:10.1038/344756a0, 1990.
- Suchy, V., Heijlen, W., Sykorova, I., Muchez, P., Dobes, P., Hladikova, J., Jackova, I., Safanda, J. and Zeman, A.: Geochemical study of calcite veins in the Silurian and Devonian of the Barrandian Basin (Czech Republic): evidence for
725 widespread post-Variscan fluid flow in the central part of the Bohemian Massif, *Sediment. Geol.*, 131(3–4), 201–219, doi:10.1016/S0037-0738(99)00136-0, 2000.
- Taillefer, A., Soliva, R., Guillou-Frottier, L., Le Goff, E., Martin, G. and Seranne, M.: Fault-Related Controls on Upward Hydrothermal Flow: An Integrated Geological Study of the Têt Fault System, Eastern Pyrénées (France), *Geofluids*, 2017, 1–19, doi:10.1155/2017/8190109, 2017.
- 730 Taillefer, A., Guillou-Frottier, L., Soliva, R., Magri, F., Lopez, S., Courrioux, G., Millot, R., Ladouche, B. and Le Goff, E.: Topographic and Faults Control of Hydrothermal Circulation Along Dormant Faults in an Orogen, *Geochemistry, Geophys. Geosystems*, 19(12), 4972–4995, doi:10.1029/2018GC007965, 2018.
- Taylor, B. D.: Stable isotope geochemistry of ore-forming fluids, in *Short Course Handbook.*, 1987.
- Travé, A., Labaume, P., Calvet, F. and Soler, A.: Sediment dewatering and pore fluid migration along thrust faults in a foreland
735 basin inferred from isotopic and elemental geochemical analyses (Eocene southern Pyrenees, Spain), *Tectonophysics*, 282(1–4), 375–398, doi:10.1016/S0040-1951(97)00225-4, 1997.
- Travé, A., Labaume, P., Calvet, F., Soler, A., Tritlla, J., Buatier, M., Potdevin, J.-L., Séguret, M., Raynaud, S. and Briquieu, L.: Fluid migration during Eocene thrust emplacement in the south Pyrenean foreland basin (Spain): an integrated structural, mineralogical and geochemical approach, *Geol. Soc. London, Spec. Publ.*, 134(1), 163–188,
740 doi:10.1144/GSL.SP.1998.134.01.08, 1998.
- Travé, A., Calvet, F., Soler, A., Labaume, P.: Fracturing and fluid migration during Paleogene compression and Neogene extension in the Catalan Coastal Ranges, Spain, *Sedimentology*, 45, 1063–1082, 1998.
- Travé, A., Calvet, F., Sans, M., Vergés, J. and Thirlwall, M.: Fluid history related to the Alpine compression at the margin of the south-Pyrenean Foreland basin: the El Guix anticline, *Tectonophysics*, 321(1), 73–102, doi:10.1016/S0040-
745 1951(00)00090-1, 2000.
- Travé, A., Calvet, F.: Syn-rift geofluids in fractures related to the early-middle Miocene evolution of the Vallès-Penedès half-graben (NE Spain), *Tectonophysics*, 36, 101–120, 2001.
- Travé, A., Labaume, P. and Vergés, J.: Fluid Systems in Foreland Fold-and-Thrust Belts: An Overview from the Southern Pyrenees, in *Thrust Belts and Foreland Basins*, pp. 93–115, Springer Berlin Heidelberg, Berlin, Heidelberg., 2007.
- 750 Travé, A., Roca, E., Playà, E., Parcerisa, D., Gómez-Gras, D. and Martín-Martín, J. D.: Migration of Mn-rich fluids through normal faults and fine-grained terrigenous sediments during early development of the Neogene Vallès-Penedès half-graben (NE Spain), *Geofluids*, 9(4), 303–320, doi:10.1111/j.1468-8123.2009.00258.x, 2009.
- Trincal, V., Buatier, M., Charpentier, D., Lacroix, B., Lanari, P., Labaume, P., Lahfid, A. and Vennemann, T.: Fluid-rock



- interactions related to metamorphic reducing fluid flow in meta-sediments: example of the Pic-de-Port-Vieux thrust (Pyrenees, Spain), *Contrib. to Mineral. Petrol.*, 172(9), 78, doi:10.1007/s00410-017-1394-5, 2017.
- 755 Turu i Michels, V. and Peña Monné, J. L.: Las terrazas fluviales del sistema Segre-Valira (Andorra- La Seu d'Urgell-Organyà, Pirineos Orientales): relación con el glaciario y la tectónica activa., *Geomorfol. y Territ. IX Reun. Nac. Geomorfología*, (January 2006), 113–128, 2006.
- Veizer, J., Ala, D., Azmy, K., Bruckschen, P., Buhl, D., Bruhn, F., Carden, G. A. F., Diener, A., Ebner, S., Godderis, Y., Jasper, T., Korte, C., Pawellek, F., Podlaha, O. G. and Strauss, H.: $^{87}\text{Sr}/^{86}\text{Sr}$, $\delta^{13}\text{C}$ and $\delta^{18}\text{O}$ evolution of Phanerozoic seawater, *Chem. Geol.*, 161(1–3), 59–88, doi:10.1016/S0009-2541(99)00081-9, 1999.
- 760 Vergés, J.: Estudi geològic del vessant Sud del Pirineu Oriental i Central: Evolució cinemàtica en 3D. PhD thesis, University of Barcelona, Barcelona., 1993.
- Vergés, J. and Fernández, M.: Tethys–Atlantic interaction along the Iberia–Africa plate boundary: The Betic–Rif orogenic system, *Tectonophysics*, 579, 144–172, doi:10.1016/j.tecto.2012.08.032, 2012.
- 765 Vergés, J. and Muñoz, J. A.: Thrust sequences in the southern central Pyrenees, *Bull. French Geol. Soc.*, 2, 265–271, 1990.
- Vergés, J., Fernández, M. and Martínez, A.: The Pyrenean orogen: pre-, syn-, and post-collisional evolution, *J. Virtual Explor.*, 08(January 2002), doi:10.3809/jvirtex.2002.00058, 2002.
- Vilasi, N., Swennen, R. and Roure, F.: Diagenesis and fracturing of Paleocene-Eocene carbonate turbidite systems in the Ionian Basin: The example of the Kelçyra area (Albania), *J. Geochemical Explor.*, 89(1-3 SPEC. ISS.), 409–413, doi:10.1016/j.jexplo.2005.11.018, 2006.
- 770 Voicu, G., Bardoux, M., Stevenson, R. and Jébrak, M.: Nd and Sr isotope study of hydrothermal scheelite and host rocks at Omai, Guiana Shield: implications for ore fluid source and flow path during the formation of orogenic gold deposits, *Miner. Depos.*, 35(4), 302–314, doi:10.1007/s001260050243, 2000.
- 775 Warren, J., Morley, C. K., Charoentitirat, T., Cartwright, I., Ampaiwan, P., Khositichaisri, P., Mirzaloo, M. and Yingyuen, J.: Structural and fluid evolution of Saraburi Group sedimentary carbonates, central Thailand: A tectonically driven fluid system, *Mar. Pet. Geol.*, 55, 100–121, doi:10.1016/j.marpetgeo.2013.12.019, 2014.
- Wayne, D. M. and McCaig, A. M.: Dating fluid flow in shear zones: Rb-Sr and U-Pb studies of syntectonic veins in the Néouvielle Massif, Pyrenees, *Geol. Soc. London, Spec. Publ.*, 144(1), 129–135, doi:10.1144/GSL.SP.1998.144.01.09, 1998.
- 780 Ziegler, P. A.: Evolution of the Arctic-North Atlantic and the Western Tethys, in *AAPG Memoir Volume 43: Evolution of the Arctic-North Atlantic and the Western Tethys.*, 1988.
- Zwart, H. J.: The variscan geology of the Pyrenees, *Tectonophysics*, 129(1–4), 9–27, doi:10.1016/0040-1951(86)90243-X, 1986.



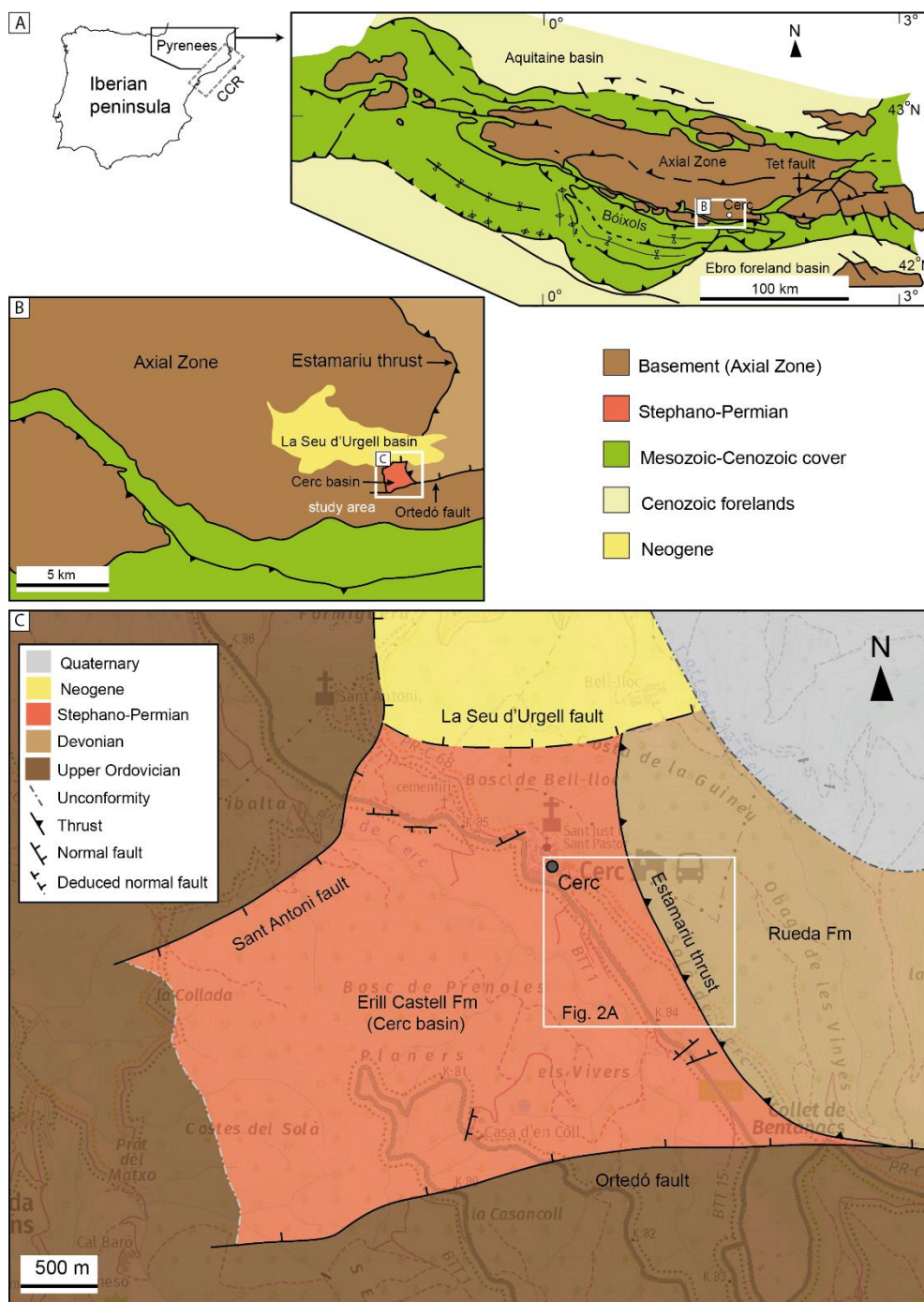
790 **Table 1.** $\delta^{18}\text{O}$, $\delta^{13}\text{C}$, $^{87}\text{Sr}/^{86}\text{Sr}$ and $^{143}\text{Nd}/^{144}\text{Nd}$ ratios of the calcite cements and related host rocks. The calculated precipitation temperature and the $\delta^{18}\text{O}_{\text{fluid}}$ of the parent fluids are also indicated. NR indicates analyzed samples in which no result was obtained.

Sample	Vein	Cement	$\delta^{18}\text{O}$ ‰VPDB	$\delta^{13}\text{C}$ ‰VPDB	$^{87}\text{Sr}/^{86}\text{Sr}$	$^{143}\text{Nd}/^{144}\text{Nd}$	Δ_{47}	T (°C)	$\delta^{18}\text{O}_{\text{fluid}}$ ‰SMOW
C9	V1a	Cc1a	-11.2	+0.91					
C8B	V1a	Cc1a	-10.7	+2					
C8A.I	V1a	Cc1a	-10.4	+2					
C8A.II	V1a	Cc1a	-10.96	+1.3	0.713018	NR			
C8A.III	V1a	Cc1a	-10.9	+1.2					
C7.I	V1a	Cc1a	-10.9	+2.1					
C7.II	V1a	Cc1a	-10.8	+0.8					
C7.III	V1a	Cc1a	-10.4	+1.96					
C4B	V1a	Cc1a	-10.3	+1.9	0.714092	NR			
C3A.I	V1a	Cc1a	-11.2	+1.9					
C3A.II	V1a	Cc1a	-11.3	+1.7					
C3A.III	V1a	Cc1a	-10.5	+1.98					
C15.I	V2	Cc2	-14.9	-1.2	0.718294	NR	0.567	56 to 98	-0.3 to -6.4
C15.II	V2	Cc2	-13.3	+0.5					
C15.III	V2	Cc2	-12.91	+1.54					
C13	V3	Cc3	-13.8	-7.1	0.714619	NR	0.445	127 to 208	+4.3 to +12.1
C12.II	V3	Cc3	-14.3	-7.3					
C10	V3	Cc3	-14.2	-9.3					
C11A	V3	Cc3	-14.2	-8.7					
C13.II	V3	Cc3	-13.6	-7.2					
C14.I	V3	Cc3	-13.4	-6.9					
C14.II	V3	Cc3	-13.7	-7.4					
C16A	V3	Cc3	-13.8	-7.2					
C16B	V3	Cc3	-14	-7					
C16C	V3	Cc3	-14.1	-6.9					
C18.I	V4	Cc4	-13.4	-7.2	0.717706		0.48	102 to 167	+0.9 to +8.1
C18.II	V4	Cc4	-13.8	-7.4					
C12.I	V5	Cc5	-8.1	-7.8	0.716923	0.512178			
C6.I	V5	Cc5	-6.7	-8.2					
C6.II	V5	Cc5	-7.4	-7.4					
C11B	V5	Cc5	-7.7	-3.8					
C3A.HR	Devonian carbonates		.5	+2.4	0.710663	NR	0.77	-5 to +3	-12.4 to -10.1
C17.HR			.51	+1.54					
C4.HR			.36	+2.7					
C11.HR	Andesites		-	-	0.743983	0.512196			

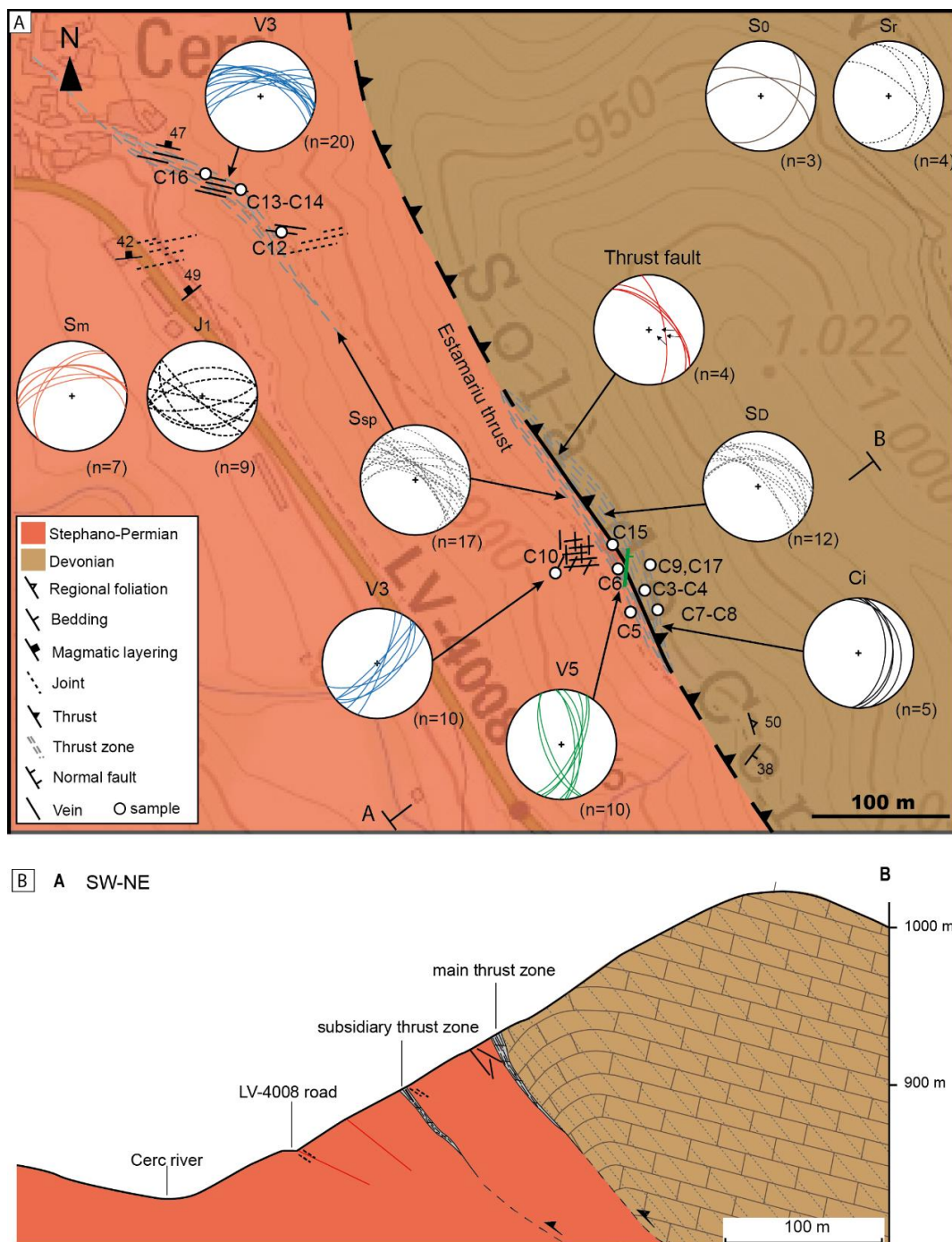


Table 2: Elemental composition (Ca, Mg, Fe, Mn, Sr) of the calcite cements Cc1a to Cc5 and host rocks from the hanging wall (HW) and footwall (FW). The scale in greens indicates higher concentrations when is darker.

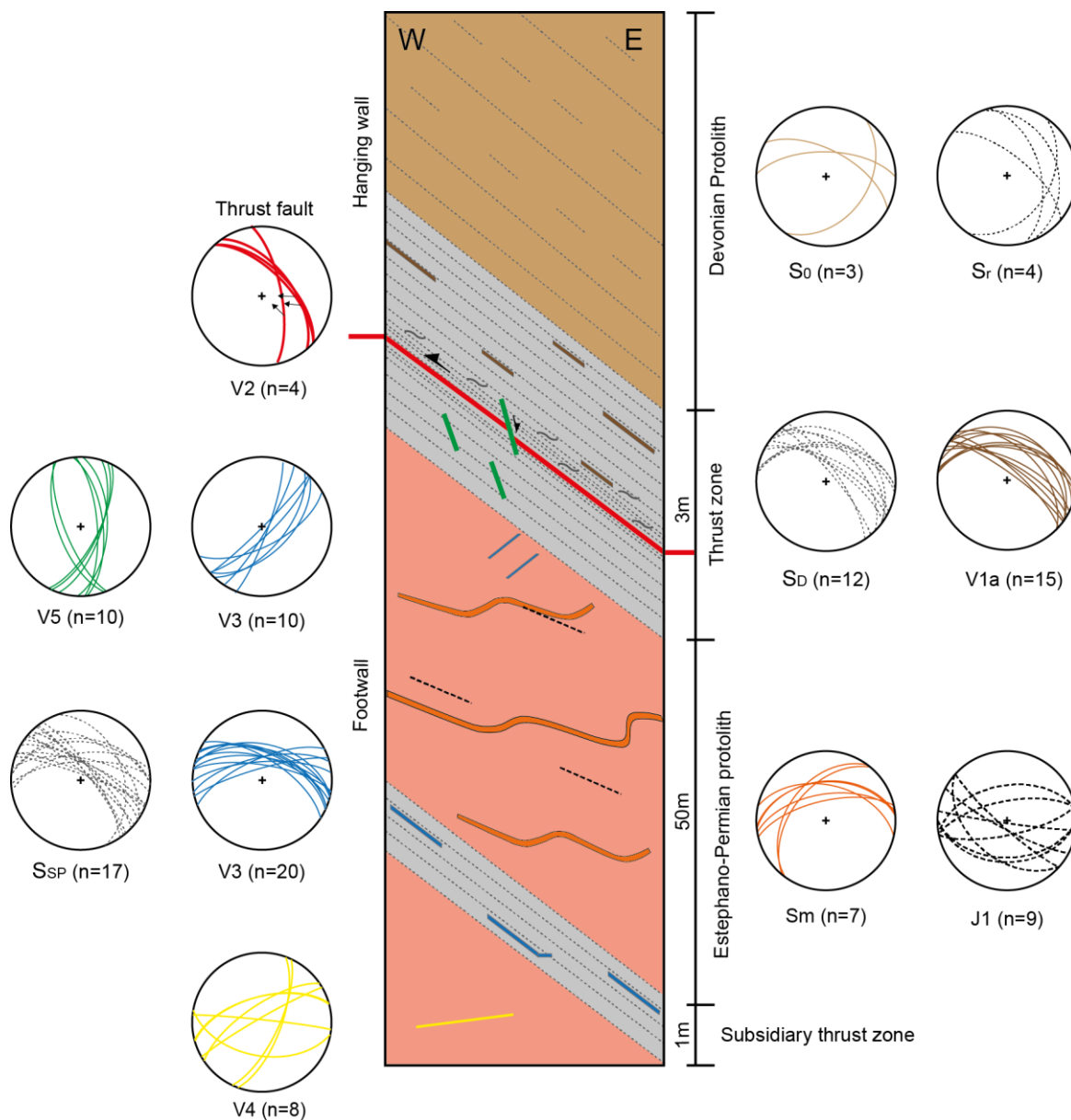
Sample	Ca ppm	Mg ppm	Fe ppm	Mn ppm	Sr ppm
Cc1a	391618	1335.9	5603.5	1243.7	543.7
Cc1a	349063	1548.6	4121.3	781.6	460.2
Cc1a	351134	1231.8	5205.4	810.3	545.5
Cc1a	337588	1126.6	3914.9	680.7	704.0
Cc2	328169	501.2	1061.4	3629.3	248.5
Cc3	364995	331.9	1647.8	8277.9	122.3
Cc3	333123	909.5	5545.9	7695.5	424.9
Cc4	333563	624.4	3814.9	4034.6	72.2
Cc5	233784	2260.0	8656.6	161.4	72.1
Cc5	281741	1626.2	4078.0	138.8	25.3
HW	320038	2752.6	6289.0	621.1	449.4
FW	4234	12830.5	43107.1	466.6	18.6



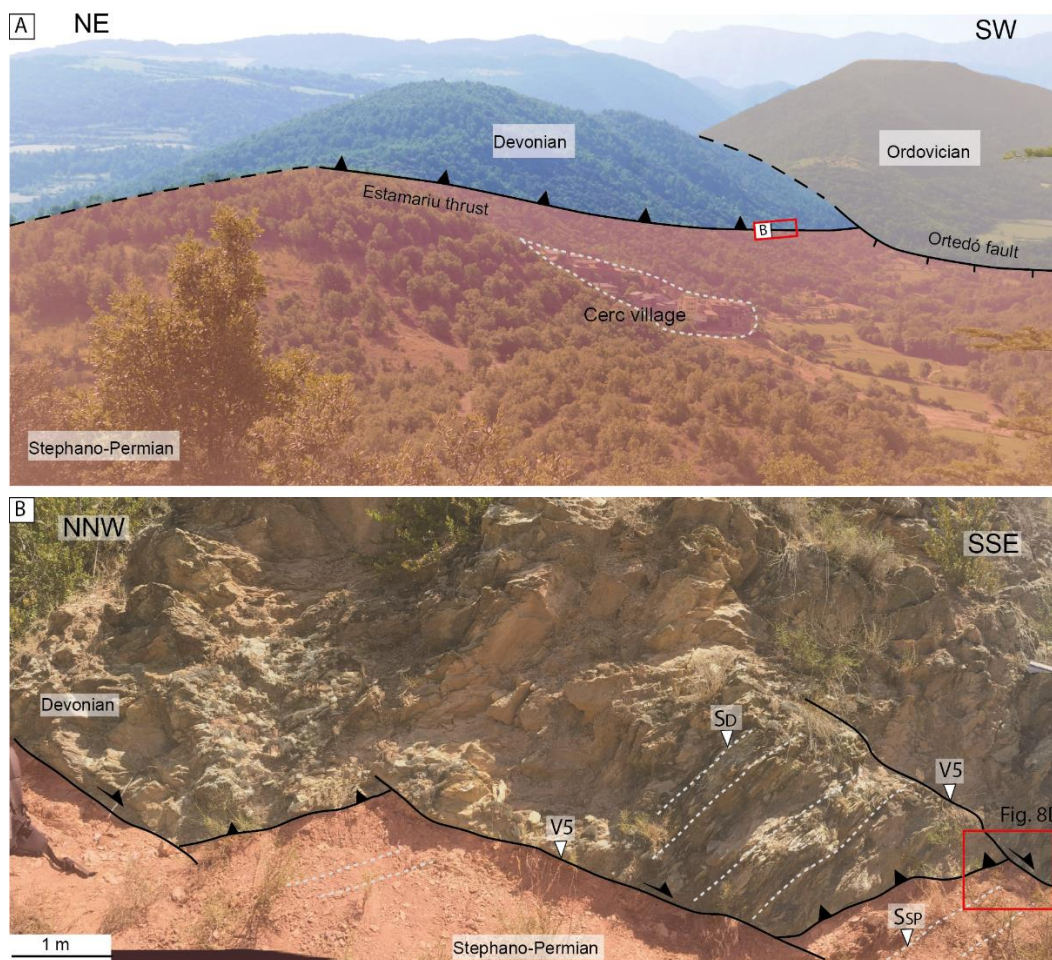
805 **Figure 1:** (A) Simplified geological map of the Pyrenees modified from (Muñoz, 2017) and its location in the Iberian Peninsula (location of the Catalan Coastal Range, CCR, is also shown). (B) Detail of the study area located within the Pyrenean Axial zone. (C) Geological map of the Cerc basin (using data from Saura (2004) and our own data) with the Estamariu thrust located in its eastern termination and the Neogene extensional faults in the northern and southern limits. The white square indicates the location of the main outcrop (Fig. 2A).



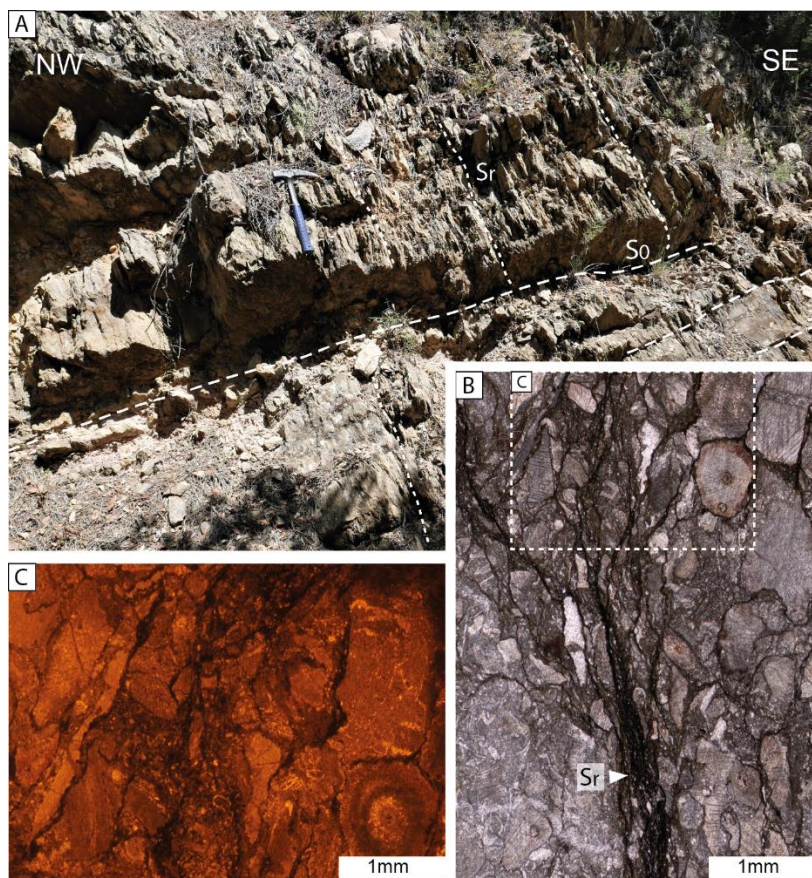
810 **Figure 2:** (A) Geological map and (B) cross-section of the Estamaru thrust, which juxtaposes a Devonian unit against a Stephano-Permian sequence (H=V, no vertical exaggeration). Lower-hemisphere equal-area stereoplots of the Devonian bedding (S₀), regional foliation (S_r), thrust zone foliation affecting the hanging wall (S_D) and footwall (S_{SP}), magmatic layering (S_m) and the different faults and veins observed in the study area are also included. Location in Fig. 1B.



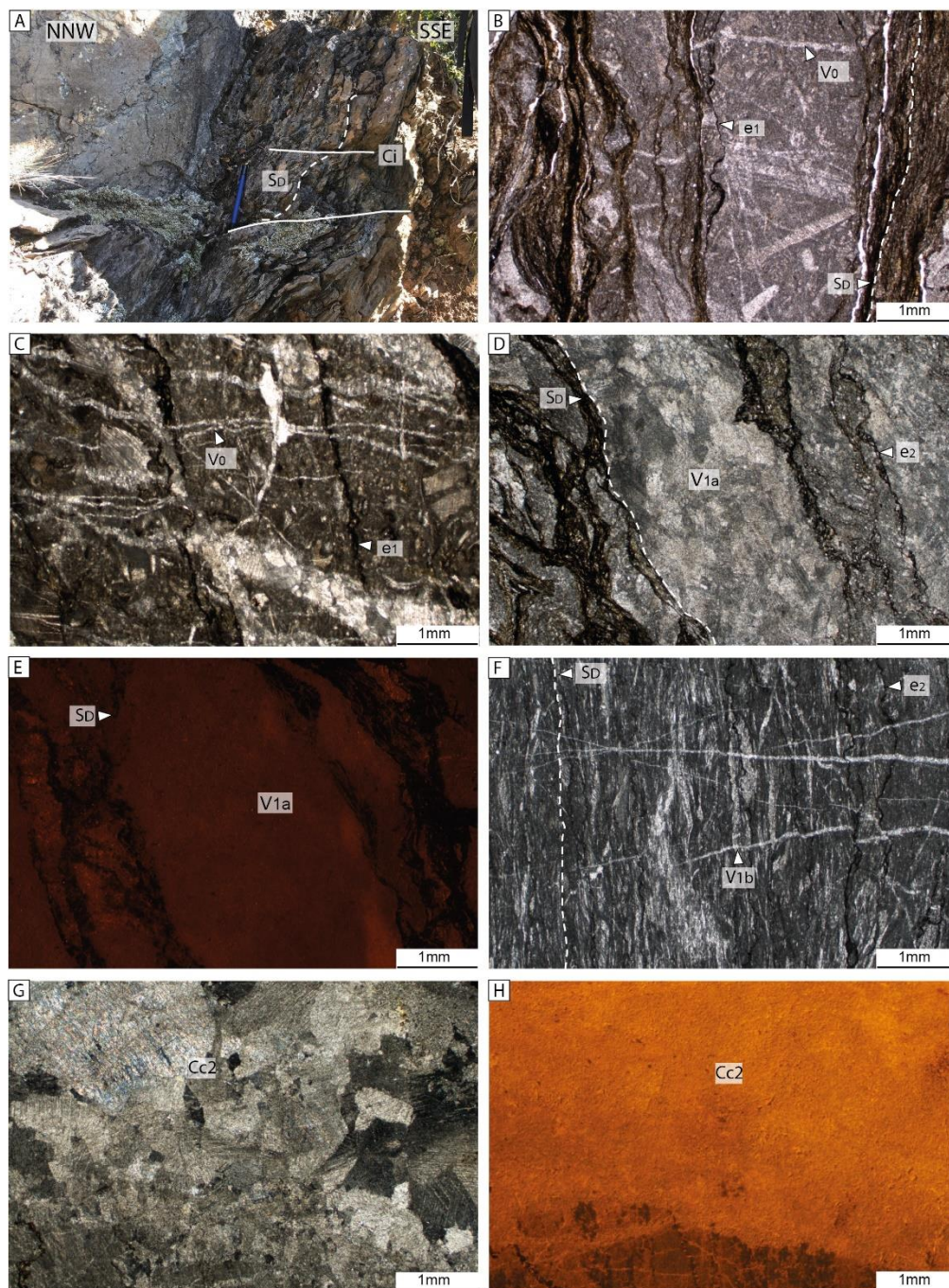
815 **Figure 3:** Sketch showing the spatial distribution of mesoscale structures within the main outcrop and lower-hemisphere equal-area stereoplots of the different mesostructures.



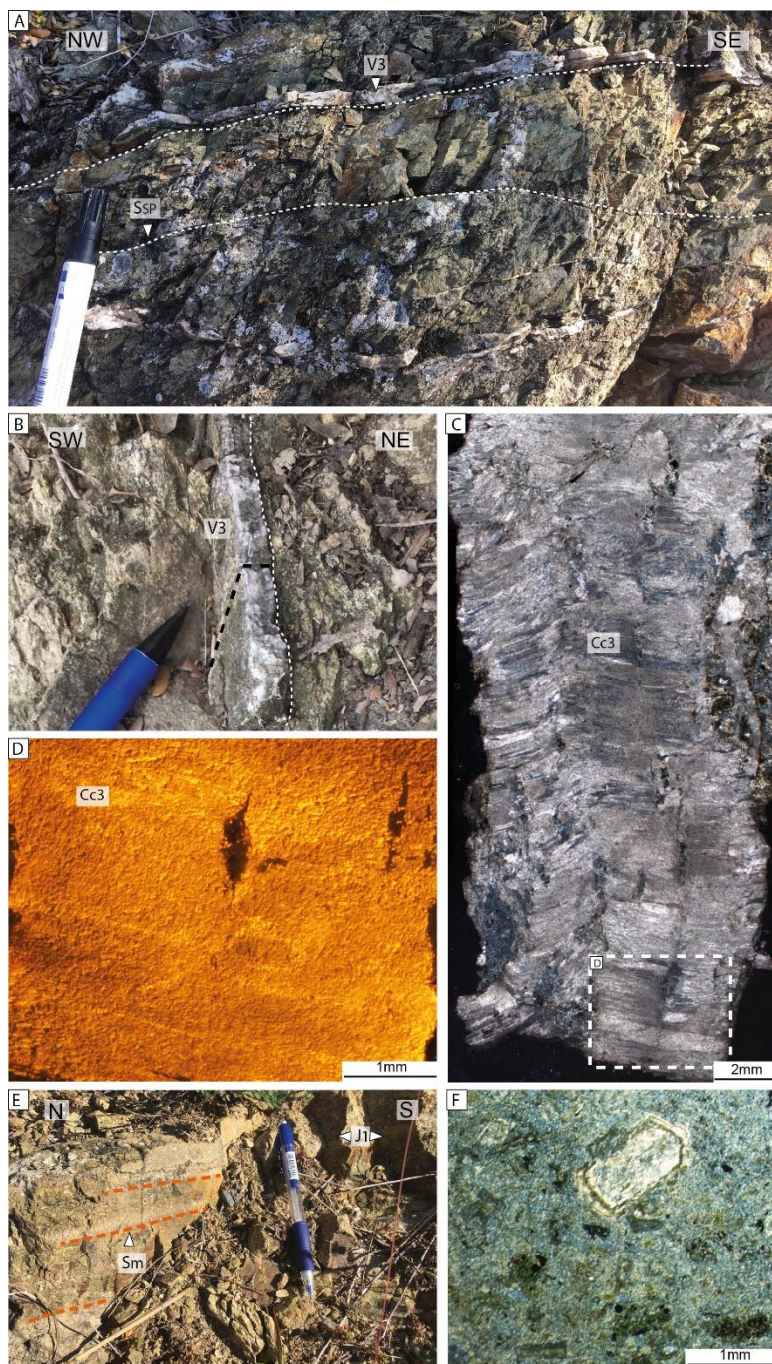
820 **Figure 4: Main outcrop of the Estamariu thrust. A) Panoramic view from the Sant Antoni hill showing the extensional Ortedó fault postdating the Estamariu thrust. B) Main outcrop showing the Estamariu thrust and the related foliation developed in the Devonian hanging wall (Sd) and in the Stephano-Permian footwall (SSP). The thrust is displaced by later shear fractures V5.**



825 **Figure 5: Devonian protolith. A) Field image showing the relationship between bedding (S_0) and regional foliation (S_r). B) Plane polarized light and C) Cathodoluminescence microphotographs of the encrinites alternating with pelitic rich bands, where the S_r is concentrated.**

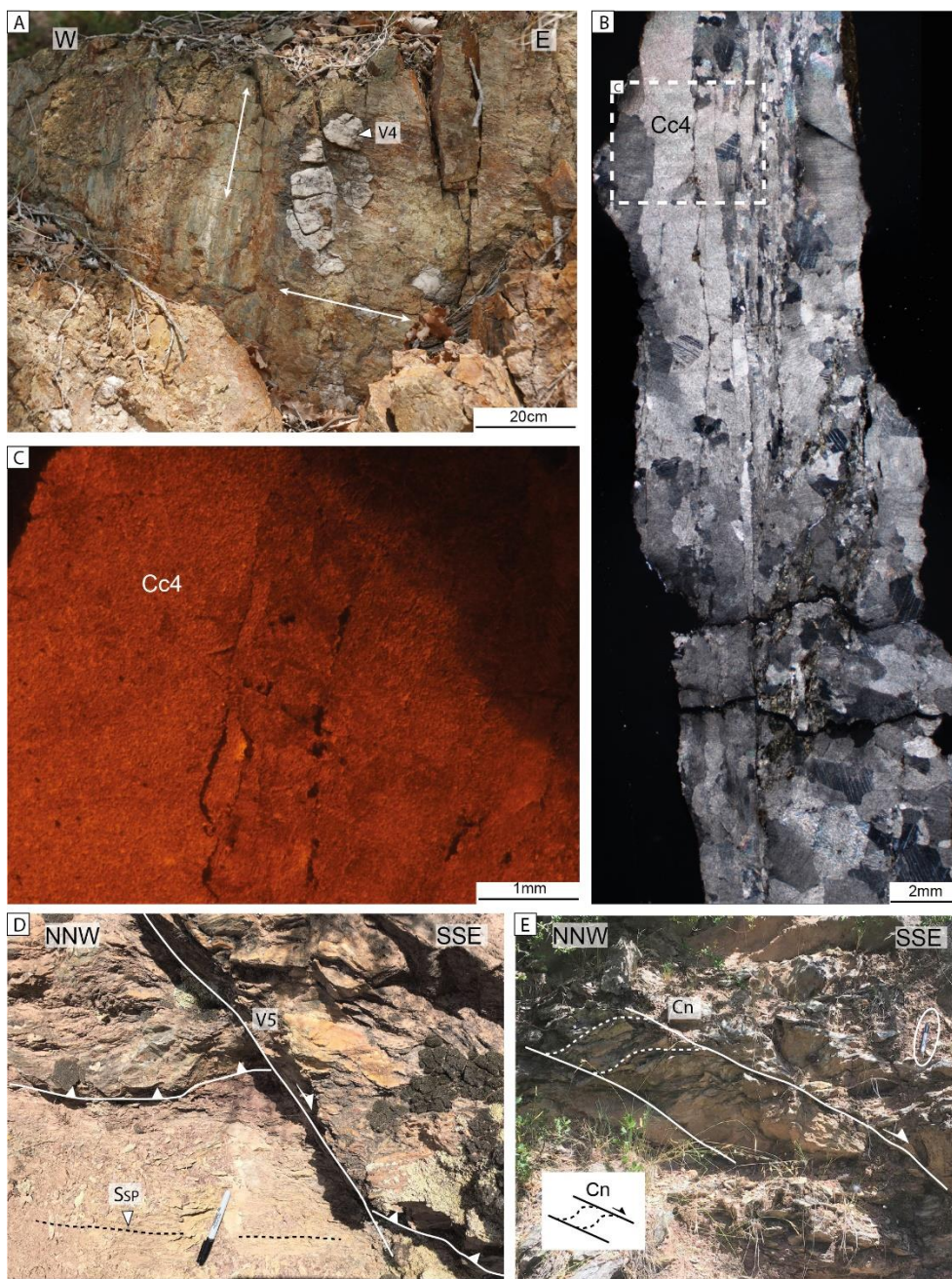


830 **Figure 6: Mesostructures and microstructures found within the thrust zone affecting the hanging wall. A) Outcrop image of the**
thrust zone foliation (S_D) and related C planes indicating reverse kinematics (C_i). Microphotographs of B) thrust zone foliation, C)
stylolites e_1 and veins V_0 affecting the Devonian encrinites, D) Crossed polarized light and E) cathodoluminescence
microphotographs of veins V_{1a} concentrated between foliation surfaces. F) Thrust zone foliation (S_D) near the fault plane and
ambiguous and perpendicular relationships between V_{1b} and e_2 . G) Crossed polarized light and H) cathodoluminescence
835 **microphotographs of calcite cement C_{c2} located on the main thrust plane (V_2).**



840

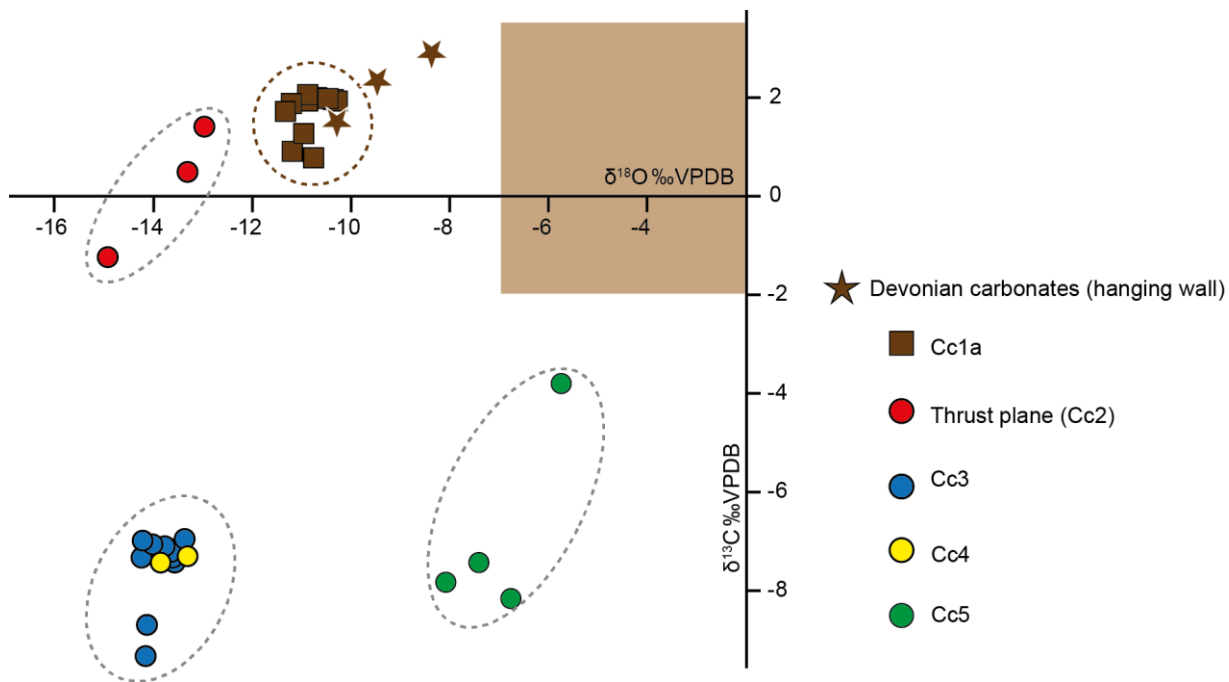
Figure 7: Mesostructures and microstructures present in the Stephano-Permian volcanic footwall. A) Field image of the subsidiary thrust zone in the footwall showing the thrust zone foliation (SSP) and the veins V3. B) Detail of veins V3 also in the subsidiary thrust zone. The black dashed line indicates the original position of the thin section observed in C. C) Crossed polarized light and D) cathodoluminescence microphotographs of veins V3, characterized by calcite fibers growing perpendicular to the vein walls (Cc3). E) Field image of the footwall andesites showing the magmatic layering (Sm) and joints J1. F) Plane polarized light microphotograph of the volcanic andesites exhibiting a porphyritic texture with a large plagioclase crystal.



845

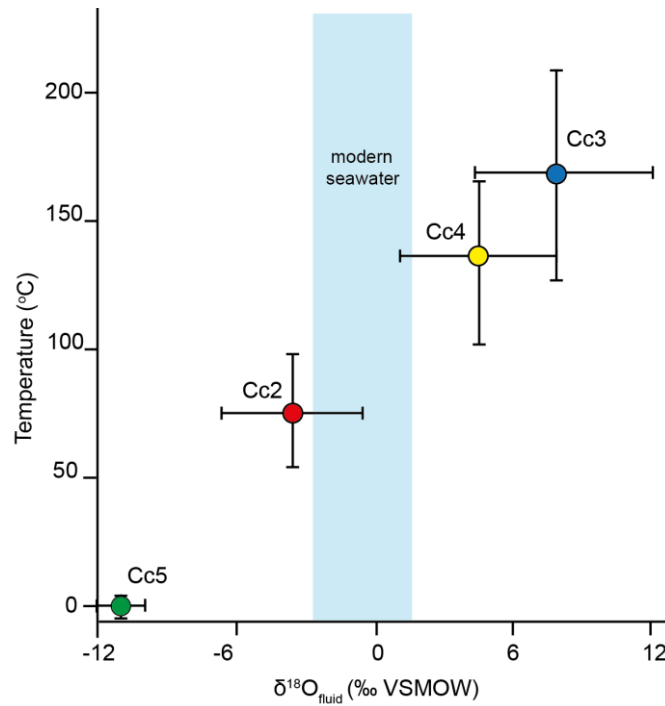
Figure 8: A) Field image of a subvertical and E-W fault plane mineralized with calcite (veins V4) and showing two striae set generations (white arrows) indicating dip-slip and strike-slip kinematics. B) Crossed polarized light and C) cathodoluminescence microphotographs of the vein-related calcite cement (Cc4). D) Shear fracture postdating the thrust zone foliation, locally mineralized with calcite veins V5. E) Shear bands (Cn) with normal kinematics located in the main thrust zone, indicating a later reactivation of the Estamariu thrust.

850



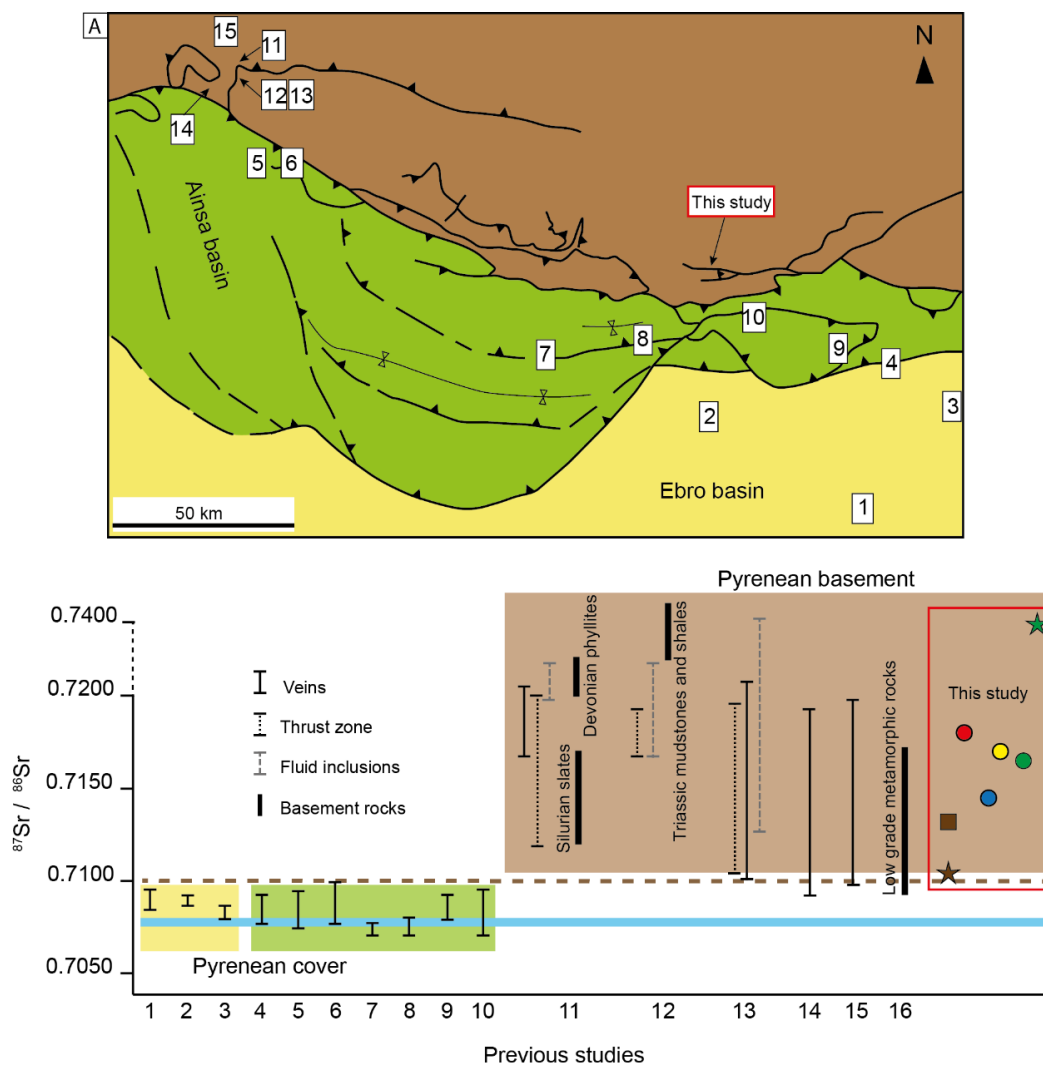
855 **Figure 9:** $\delta^{18}\text{O}$ and $\delta^{13}\text{C}$ values of calcite cements Cc1a to Cc5 and the Devonian carbonates from the hanging wall. The brown box
refers to typical values of Devonian marine carbonates (Veizer et al., 1999).

860



865

Figure 10: Temperatures (°C) vs $\delta^{18}\text{O}_{\text{fluid}}$ calculated for cements Cc2 to Cc5. The typical $\delta^{18}\text{O}$ values for modern seawater (blue band) are from Veizer et al., (1999).



870

875

880

Figure 11: Simplified geological map of the south-central Pyrenees showing the location of structures where $^{87}\text{Sr}/^{86}\text{Sr}$ analysis have been carried out. Below, $^{87}\text{Sr}/^{86}\text{Sr}$ ratios from this study compared to results from other structures involving either cover units (1-10) or basement rocks (11-16). The blue thick line refers to the $^{87}\text{Sr}/^{86}\text{Sr}$ range of Phanerozoic seawater and the dashed brown line represents the $^{87}\text{Sr}/^{86}\text{Sr}$ limit value between basement and cover structures. 1. El Guix anticline (Travé et al., 2000), 2. Puig Reig anticline (Cruset et al., 2016), 3. L'Escala thrust (Cruset et al., 2018), 4. Vallfogona thrust (Cruset et al., 2018), 5. Ainsa basin (Travé et al., 1997), 6. Ainsa-Bielsa area (McCaig et al., 1995), 7. Minor Bóixols thrust (Muñoz-López et al., under review), 8. Bóixols anticline (Nardini et al., 2019), 9. Lower Pedraforca thrust (Cruset, 2019), 10. Upper Pedraforca thrust (Cruset, 2019), 11. Gavarnie thrust (McCaig et al., 1995), 12. Pic de Port Vieux thrust (Banks et al., 1991), 13. Pic de Port Vieux thrust (McCaig et al., 2000b), 14. Plan de Larri thrust (McCaig et al., 1995), 15. La Glere shear zone (Wayne and McCaig, 1998). 16. Trois Seigneurs Massif (not in the map) (Bickle et al., 1988).

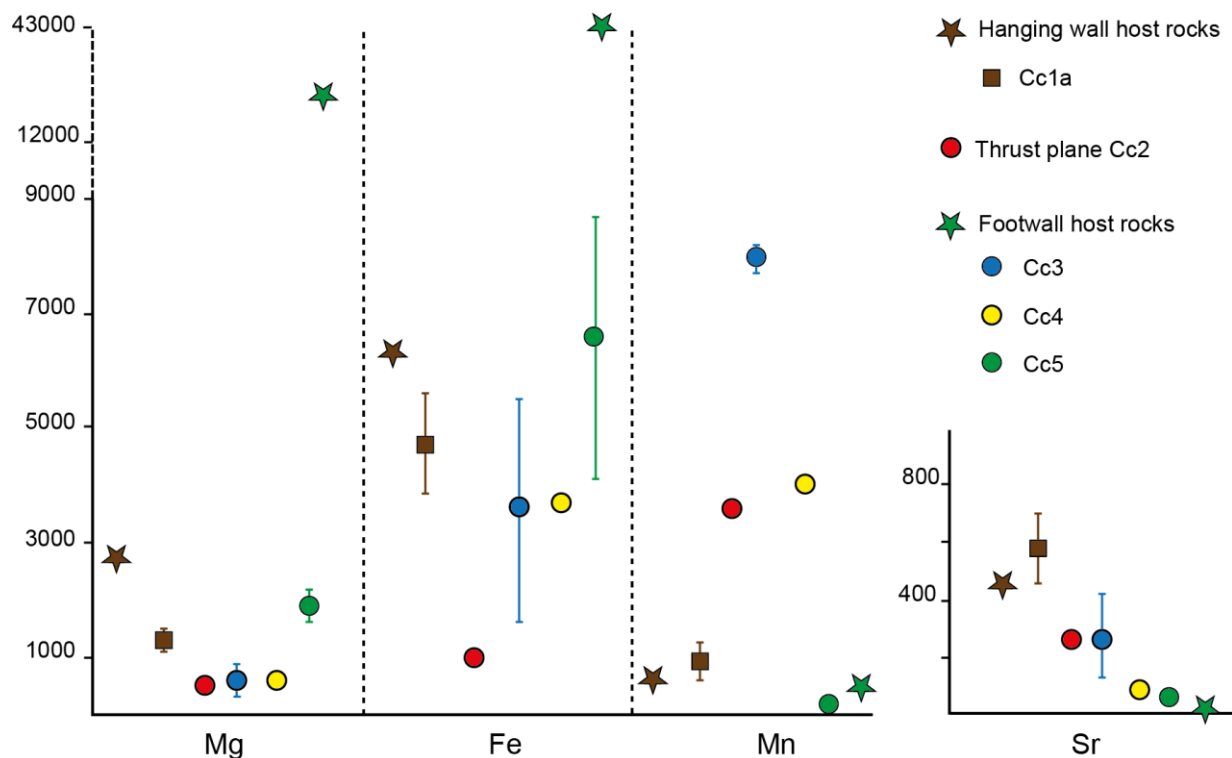


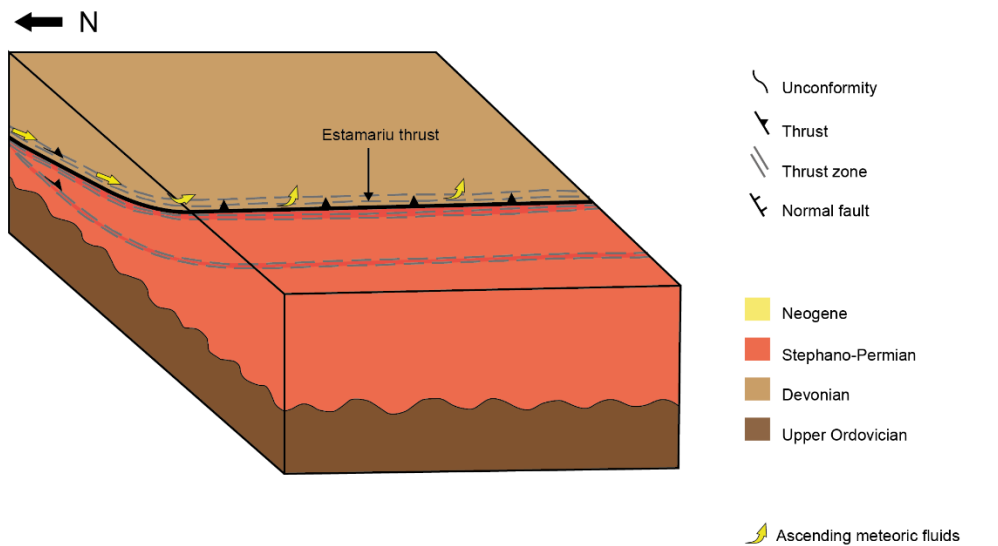
Figure 12: Elemental composition (including Mg, Fe, Mn and Sr) in ppm of the different calcite cements and host rocks. Bars indicate maximum, minimum and average composition.

885



A Alpine compression

Reactivation of the Estamariu thrust
 Calcite cements Cc1a and Cc2



B Neogene extension

Reactivation of the Estamariu thrust and development of normal faults
 Calcite cement Cc3, Cc4 and Cc5

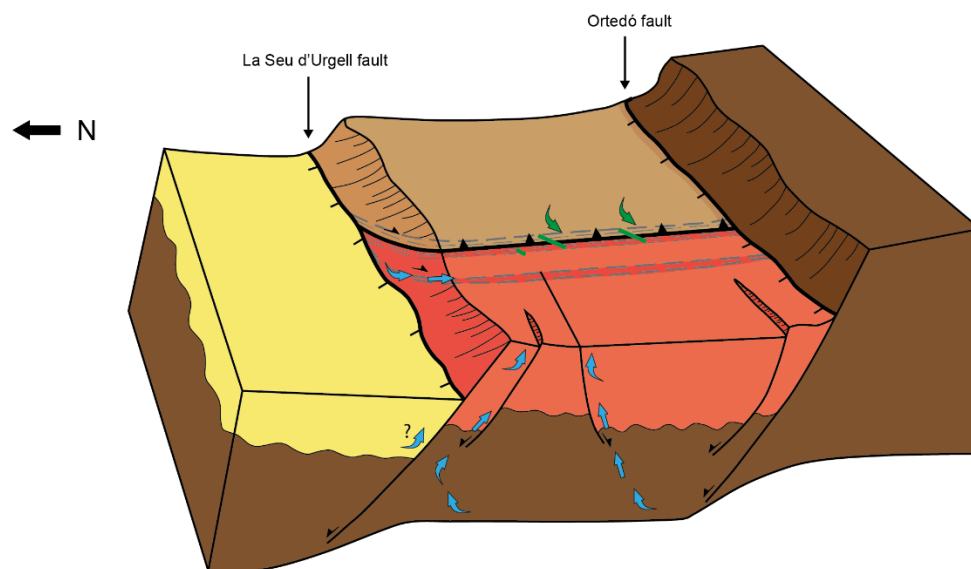


Figure 13: Tectonic evolution of the study area (not to scale) and relationship with the evolution of the fluid system. A) During the Alpine reactivation of the Estamariu thrust, a meteoric fluid (yellow arrows) interacted at depth with basement rocks and then migrated channelized along the fault plane towards the hanging wall, precipitating cements Cc1a and Cc2. B) During the Neogene extension, basement-derived hydrothermal fluids (blue arrows) flowed upwards through newly formed and reactivated fault zones. This fluid precipitated calcite cements Cc3 and Cc4. Finally, during ongoing deformation, meteoric fluids (green arrows) percolated in the system and precipitated Cc5.

890